SPAM

Submergence Plane Analysis and Modeling for a Fast Current Oil Containment Barrier

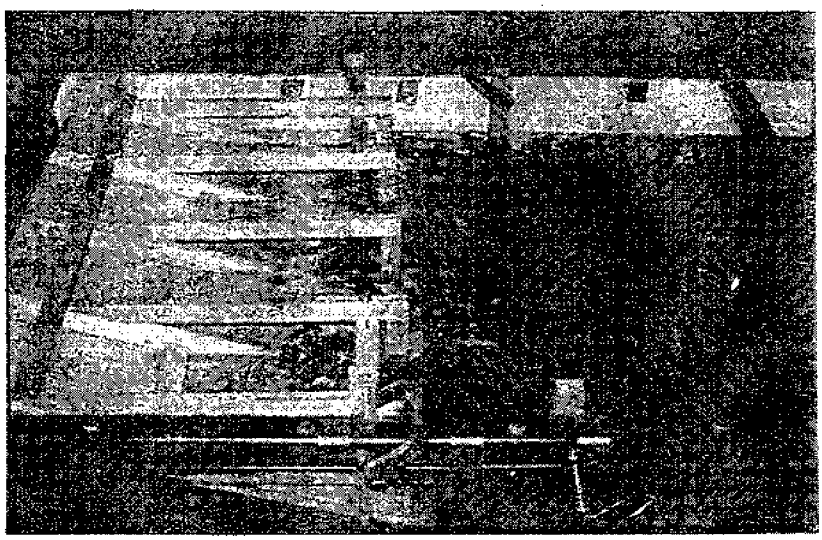

Tech 797 UNH Ocean Projects
Engineering Senior Design
1999 – 2000

Project Members:
Brett Fullerton
Richard Roman

Project Advisor:
Dr. M. Robinson Swift

Report submitted:
April 21st, 2000

Sea Grant
New Hampshire/Maine

S.P.A.M.

Submergence Plane Analysis and Modeling for a Fast Current Oil Containment Barrier

By:

BRETT FULLERTON
and
RICHARD ROMAN

Mechanical Engineering
University of New Hampshire

Tech 797 Ocean Projects
Engineering Senior Design
1999 - 2000

Acknowledgements

"This work is the result of research sponsored in part, by the National Sea Grant College Program, NOAA, Department of Commerce, under grant #NA96RG0102 through the University of New Hampshire / University of Maine Sea Grant Program."

Many thanks go out to the following people, who helped us with assistance and support throughout the project:

Dr. M. Robinson Swift, for your advise and guidance through the project and for taking the time to photograph each of the bead experiments. The project would not have been possible without your expertise.

Robert Steen, for answering an endless amount of questions, for your support, and for operating the flume through all of the bead testing experiments, even on a Sunday.

John Scott, for your general support and financial management of our budget.

Michael Palzynski, for letting us use the ten-pound load cell and for taking the time to teach me how to use it and the program that goes along with it.

The Ocean Engineers who gave their support and help, whether it was help finding equipment in the lab, photographing or video taping our experiments or for simply being silly making our work more enjoyable. Thanks: Dave Fredriksson, Pat Dugan, Peter Norse, Derek Michelin, Laura Cavagnaro, and Borgan Morton.

TABLE OF CONTENTS

List of Tables

List of Figures

Abstract

Submergence Plane Analysis and Modeling

by

Brett Fullerton and Richard Roman
University of New Hampshire, May, 2000

This report covers a yearlong study and analysis of an oil spill containment device known as the "Bay Defender" using the submergence plane containment concept. The purpose of the study was to analyze the current submergence plane design and research alternative plane shapes with the hope that future designs can improve oil retention percentages for fast moving currents.

The study consisted of creating near half scale models of various submergence plane designs, which were then tested in the University of New Hampshire's recirculating flume tank. Lift and drag tests, fluid flow measurements, and bead retention experiments were performed on the two-dimensional scale models. Results show a strong benefit in changing the submergence plane shape to improve dynamic fluid flow on the plane, thereby increasing oil containment at high current speeds.

CHAPTER 1

INTRODUCTION

Purpose

Oil spills are an inevitable consequence of the high demand the world has today for oil consumption. Conventional oil booms like those found standard in the oil transportation industry, have been an important tool in oil spill recovery. These containment booms are, however, limited by moving water, everyday tidal currents in particular. The failure of an oil boom occurs when the perpendicular component of the current speed exceeds a critical value, which has been determined to be between 0.6 and 1.0 knots, depending on the type of oil. Many of the major shipping ports and harbors can experience tidal currents daily that exceed this critical value, thus posing a serious threat to the surrounding coastal environments.

Previous work by the University of New Hampshire and other groups have lead to the development of a flexible oil barrier and containment device, known as the "Bay Defender". This device has shown that it can successfully collect floating oils in currents nearly three times the speed, at which, conventional oil booms leak. Although this device, if implemented, would be a major improvement to existing techniques, through refinement, the submergence plane oil containment system shows promising signs of retaining oil at even greater current speeds.

The purpose of this yearlong project was to study the fluid dynamics around submergence planes of varying shapes with the intention of improving containment

performance even further. Focus areas were quantifying the lift and drag effects, the flow inside the containment region, and comparisons of the retention percentages for various submergence plane designs. Through these experiments, future submergence plane designs can be modified to eliminate certain shortfalls, making the "Bay Defender" idea more plausible for both New Hampshire's seacoast, as well as other waterfront communities.

Previous Work

The conventional oil boom, seen in the media from the Exxon *Valdez* accident of 1989, are standard clean-up equipment for the oil industry. The concept behind these containment devices is that a floating curtain will collect or gather the oil slick floating on the surface of the water. For calm waters with no current, the booms perform exceptionally well; however, for many places where tidal currents are present, the booms often fail, meaning oil spillage. Numerous tests have shown that the critical velocity perpendicular to the booms is between 0.6 and 1.0 knots, depending on the type of oil, its density and viscous properties. This is a significant limitation since many ports and harbors have tidal currents that easily exceed these speeds. The possibility of towing such a boom with a vessel is also severely compromised, since most ocean-going ships require speeds greater than one knot on the rudder for maneuverability and steerageway.

Vertical barriers or oil booms usually consist of three parts; a large foam float to remain on the water's surface, a curtain material to create the barrier, and a weight at the bottom to keep the curtain submerged and vertical in the water. A considerable amount

of work has been performed on the failure of vertical barriers by researchers like Wicks (1969), Agrawal and Hale (1974), Milgram and van Houton (1978), and Delvigne (1989). Since there are many different types of oil, which come in varying grades and densities, there are also different methods of boom failure.

The lighter, lower viscosity oils have been shown to fail by generating of oil/water interface waves, which grow, become entrained in the flow and are carried underneath the curtain. (Coyne, 1995) On the other hand, the heavier oils, as described by Delvigne (1989), build in height, H, as the length of the slick, L, decreases. (see Figure 1) The building up of more oil occurs, until eventually the oil passes underneath the curtain. This is known as entrainment failure.

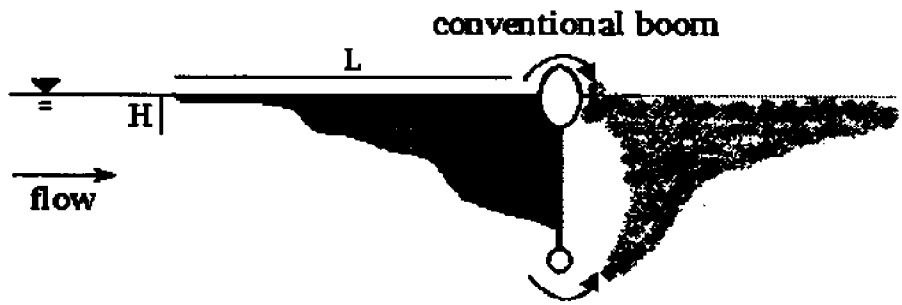

Figure 1: Diagram of Conventional Boom Failures

The failures of the conventional boom support the need for a mechanism other than a single wall barrier. The submergence plane theory avoids these types of failure by not exposing the conventional boom perpendicularly to the current's flow. Earlier, research performed by Bianchi and Henry (1973) showed that the submergence plane concept could successfully hold oil at speeds above two knots. Also, companies like JBF Scientific Inc. and LPI Corp. researched the concept further, although typically in applications for oil skimmers, which were towed behind or side-by-side by ships. (Coyne,

1995) Projects at the University of New Hampshire have focused on flexible barriers rather than hard-structure (steel), narrow skimmers. Prototypes from the University of New Hampshire have been designed for anchoring against the strong currents found in the Piscataqua River of Portsmouth, N.H..

Figure 2: Submergence Plane Containment Concept

The concept of the submergence plane system in Figure 2 operates by forcing the oil slick down the inclined surface called the submergence plane (A), where it hits the inlet gap, which is created between the submergence plane (A) and the horizontal baffle (B). Once past the gap, the oil floats back to the surface of the water, since the oil is less dense than water, and remains inside the containment volume of the device. At the back of the device is a rear boom (C), which encloses the entire system. The horizontal baffle (B) has two functions; first, it separates the contained region from the incident flow, therefore, eliminating entrainment failure as described by Delvigne (1989) and second, the horizontal baffle allows any excess water that may have entered the containment region to escape out the back through a number of exit holes.

The submergence plane concept of oil collection does not, however, try to make conventional booms obsolete, since they do perform well in low current speed conditions, but rather, it incorporates the traditional boom into the setup. The configuration of the

Bay Defender in Figure 3 actually uses hundreds of feet of boom to funnel the oil slick into an apex, where the Bay Defender collects the oil (see Figure 4).

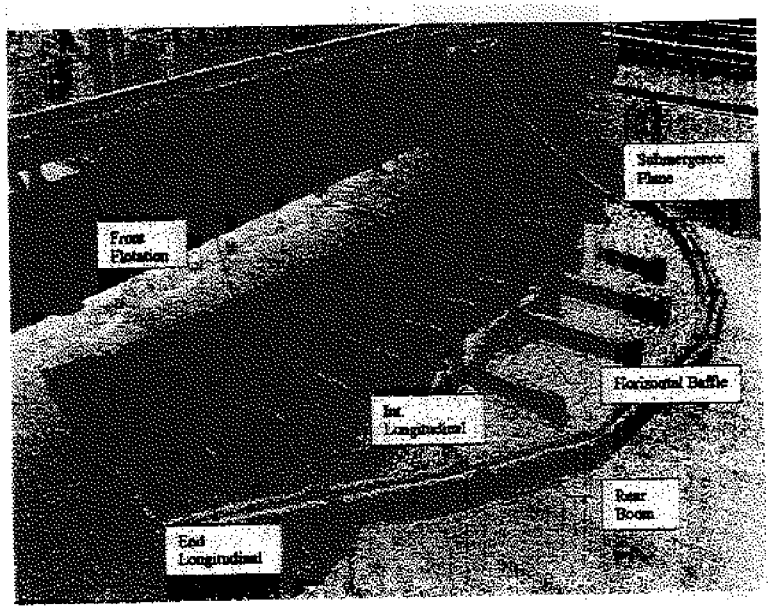

Figure 3: Labeled Picture of the 1997 "Bay Defender" Prototype (Diprofio, 1998)

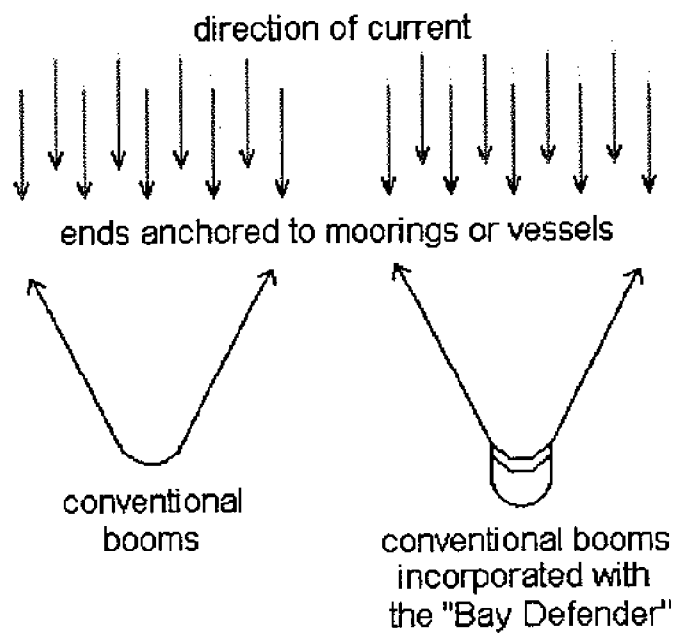

Figure 4: Diagram of Funneling to the Apex

This system, using the booms, works well, since the perpendicular component of the current's velocity never exceeds the critical velocity of the booms and, therefore, never allows any excess oil to accumulate at the booms. The bulk of the oil is forced to the apex, where it is scooped up by the Bay Defender submergence plane.

One limiting factor keeping the Bay Defender from performing better at even higher current speeds is the dynamic effect the entire device experiences causing it to lift or "plane" from the water. When this occurs, the submergence plane rises out of the

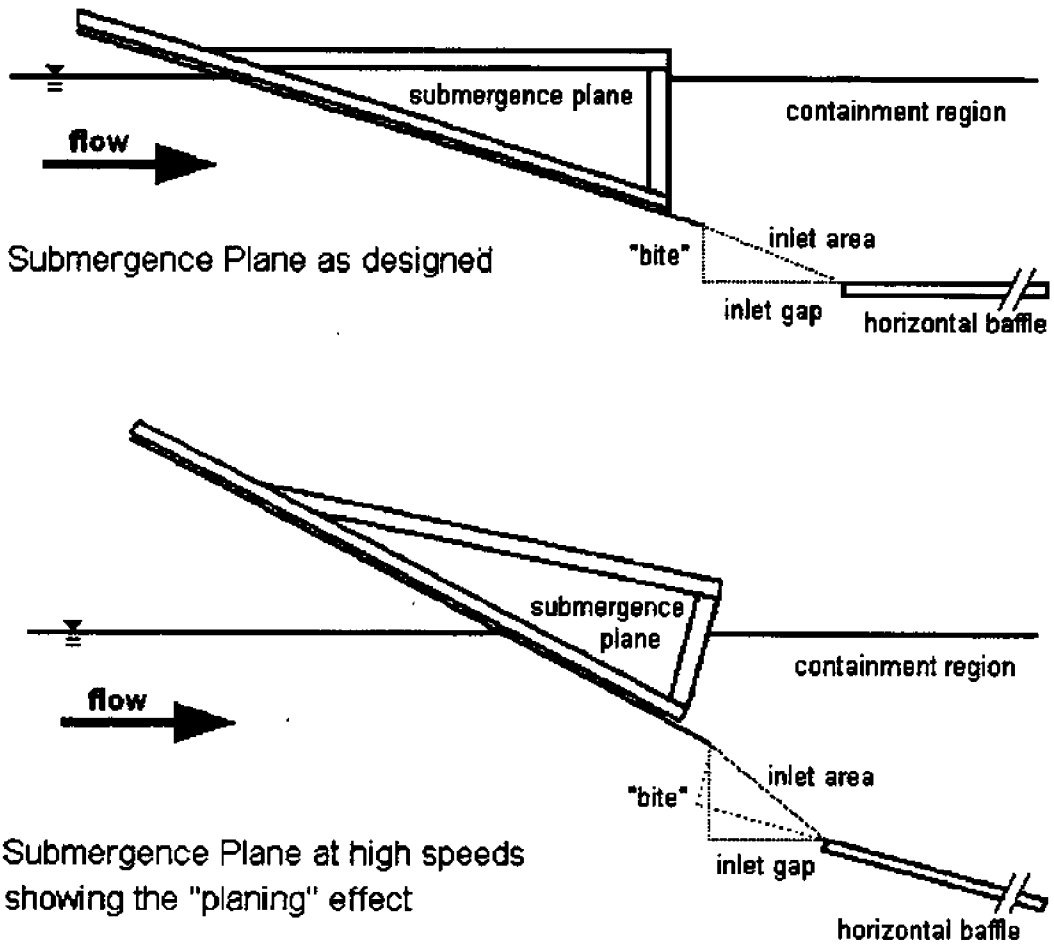

Figure 5: Diagram of the Dynamic Effects on the Submergence Plane

water, similar to the effect a speed boat has as it accelerates from a low speed. This dynamic "planing" effect naturally changes the submergence plane's angle of attack and

inlet gap geometries, particularly the inlet opening known as the "bite". Figure 5 shows how the submergence plane is supposed to sit in the water and what happens as it "planes". (notice the change in size of the bite area)

A second limitation to the submergence plane's oil-collecting efficiency is an inherent problem due to the nature of the submergence plane's construction. For simplicity in deployment, the Bay Defender must be packable, easy-to-setup, and quick to deploy. For this reason, the Bay Defender uses a flexible urethane material for surfaces connected to independent, floating, aluminum truss supports. Since the urethane fabric shape is not fully supported to its straight shape, the material bows or "cusps" in a convex-up shape due to the force of the water pushing on the material. This tendency has a strong negative effect on the containment of oil, since much of the oil traveling down the submergence plane may actually shoot past the inlet gap, thus missing the containment region. This effect only gets worse as the water's current velocity increases. It is, however, a "catch-22" situation, since the Bay Defender must be able to pack small for ease of transporting, yet the submergence plane needs to keep its shape better to remain as effective. Although the submergence plane would clearly perform better, if it were rigid, this is not an option, unless it could still pack well.

The ideal shape of the submergence plane is believed to be a concave-up shape because it would reduce the vortices produced at the trailing edge of the plane. Any turbulence present in the area certainly affects the amount of oil finding its way into the holding volume. A problem arises in how to design and manufacture such a shape, while maintaining the same transporting capability of the Bay Defender, so that the device can easily be deployed at the site of a spill.

Objectives

The specific objectives of the project were to:

1) Determine and compare the lift and drag forces of three submergence plane designs.
2) Measure the flow of water through the containment regions of each of the three submergence plane designs.
3) Compare bead retention capability for the three submergence plane shapes.

Approach

The central approach to achieving these objectives was to create three two-dimensional models of the Bay Defender prototype, varying the submergence plane shape with each design. Three radically different submergence plane shapes were selected for comparison purposes. These shapes included a straight plane, a convex-up plane, and a concave-up plane. Each submergence plane shape was selected for a specific reason, which will be outlined in the next chapter.

In order to determine the lift and drag forces of the submergence plane, a load cell was used to find the horizontal force (see Figure 6) required to hold the plane in place, as the water pushed on it. The submergence plane was allowed to move in the horizontal direction, as well as, pivot through wheels, which were attached to the front end. The tracks retaining the wheels would not allow the plane to move vertically in the

recirculating flume tank. Since the draft of the submergence plane would rise as the flow increased, weights were added to the back of the submergence plane to keep it at the desired draft. This allowed for the lift and drag forces to be calculated through the summing of forces and moments at equilibrium. Lift and drag forces would be determined for varying current speeds with the three submergence plane models.

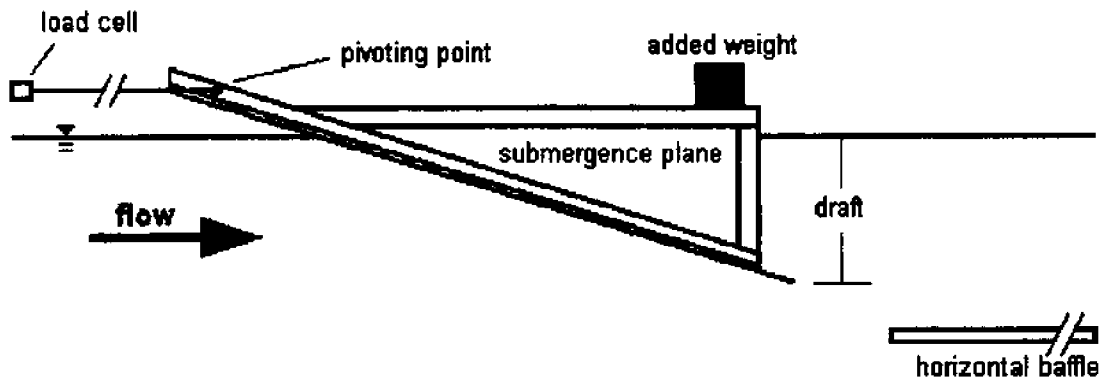

Figure 6: Diagram of Lift and Drag Setup

The second objective was to measure the flow of water in the containment region with the use of an electromagnetic flow meter. The inlet area and bite remained equal for each of the submergence plane designs, though, the nature of the different submergence plane shapes either made the containment region turbulent or stagnant. Various positions in the containment region were tested to observe the way the flow of water entered and exited the system. Four positions in the containment region were tested. These positions included upper and lower measurements just in front of the exit holes of the horizontal baffle and inline with the tail end of the baffle. From these measurements, a comparative analysis of the different plane shapes can be made.

The third and final objective of the study was to perform comparative retention experiments. Plastic beads were selected for retention experiments, instead of oil, since

the beads mimicked real oil without the hazardous handling and messy clean-up. The beads chosen had the same specific gravity as Sundex oil, a heavy oil with a high specific gravity. A known volume of beads was added to the flow to observe and quantify which submergence plane design was likely to hold the most beads. The volume contained and lost were compared in percentages to the initial volume added to the flume.

CHAPTER 2

TESTING FACILITIES

Experiments were performed in the recirculating freshwater flume located in the Jere Chase Ocean Engineering Building. The flume tank was designed and constructed by Doane (1994) and dedicated for the use of oil spill research. Recent improvements were made on the flume, which included doubling the tank's width, as well as adding ducts to smooth the turbulent flow. The flume tank has the dimensions of forty feet in length, forty-six inches wide and roughly four feet tall with a water depth of thirty inches (see Figure 7 for a schematic of the flume). One side of the flume tank is made with acrylic panel to allow for visual observations during testing. The current flow is created by two counter-rotating propellers, powered by two 20 hp electric motors, which can create a current speed just under two knots. The speed of the electric motors is regulated by a variable frequency driver, which takes input frequencies from zero to sixty Hertz with a tenth of a Hertz variability.

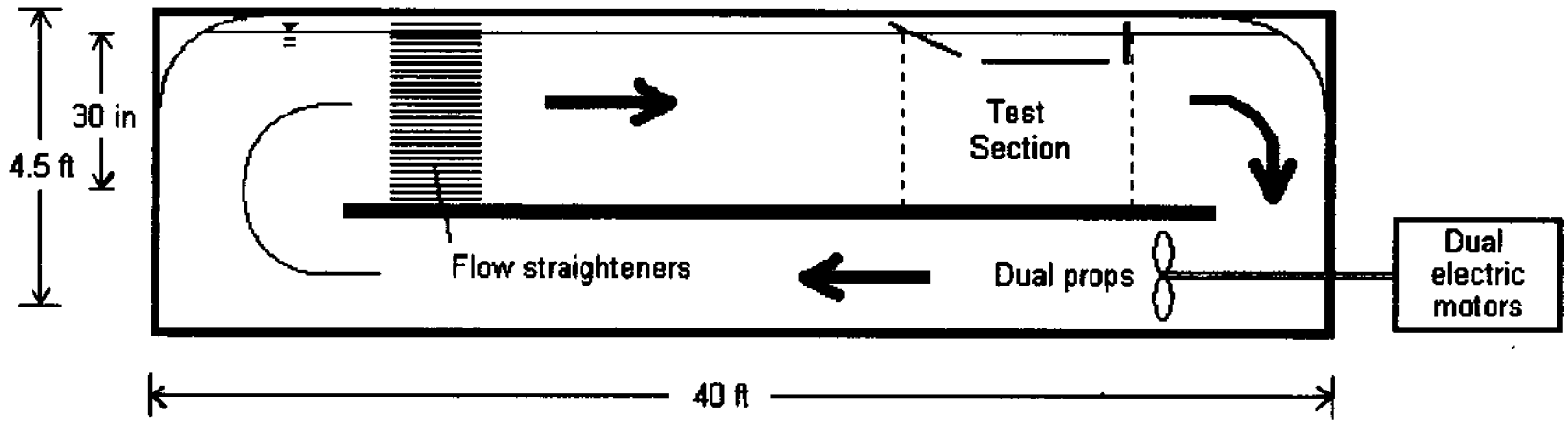

Figure 7: Schematic of the Recirculating Flume

CHAPTER 3

Model Design and Construction

The starting point of the project was to determine the submergence plane shapes, which were to be modeled and tested for the comparisons. Three radically different shapes were selected, since they would show a distinct contrast to each other. Presently, the working prototypes, such as the Bay Defender use a straight submergence plane, therefore, it was clear to create one design from what is presently being used (see Figure 3).

The second plane shape selected was based on the problem experienced by the urethane surface material "cusping", due to the force of the water. It was clear from watching videos of previous testing that this undesired shape negatively affects the retention capabilities of the oil entering through the inlet area (refer to Figure 5). Much of the oil traveling down the submergence plane would slip past the inlet area, never having a chance to rise. It was decided to create this shape as our second model to investigate how an undesirable cusp in the submergence plane would affect the experimental results. This downwards-curved shape was coined the "convex" plane, since it had an arch-like appearance (see Figure 8).

The third submergence plane design was based on the idea that a better design would be to curve the end of the plane upwards, so there is flow into the containment region. This design would reduce the number of vortices produced at the trailing edge of the plane allowing oil to rise to the surface undisturbed by the water's flow. Small amounts of turbulence present in the inlet area certainly affects the amount of oil finding its way into the containment volume. This shape was previously dubbed the "J" plane,

but because of its obvious shape, it will be referred to as the "concave" plane throughout the project (see Figure 8)

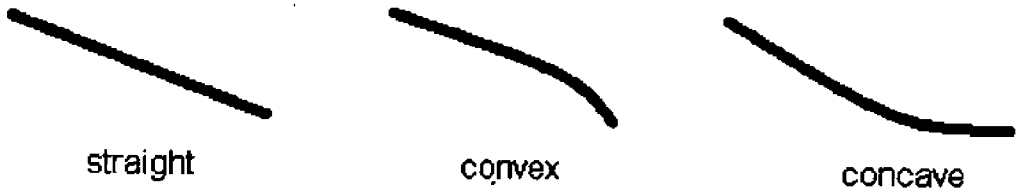

Figure 8: Plane Shape Terminology

Once the general plane shapes were chosen, design and construction could begin. There were two factors to consider in the design of the submergence planes. The first was a desire to be at half-scale of the Bay Defender prototype in order keep scaling factors as simple as possible for future analysis. The second influencing factor was the size of the recirculating flume tank, in which the testing was to take place. The idea was to maximize the usable amount of test space.

A standard guideline for scaled modeling in naval architecture is for the model's draft to be one-hundredth the depth of the test section (one fiftieth for less precise modeling). If the draft-to-depth ratio is any smaller than this, the data obtained from testing could be skewed due to reflected waves or boundary layers. Since the recirculating flume has a maximum depth of roughly thirty inches, this would mean the model's draft would be less than an inch, which is unacceptable. Since the tests performed were for comparative purposes, this scale modeling guideline was disregarded. A draft limitation of roughly six inches was setup to insure sufficient cross-sectional area for the flow of water to squeeze through. All submergence plane models were to maintain a five-inch draft thus resulting in a five twelfths (or 0.417) scale to the Bay

Defender specifications. This was an undesirable scale, but necessary, due to the flume's dimensions.

The next section divides the design and construction of the models into separate components that make up the Bay Defender prototype. These components include: the submergence plane, the horizontal baffle, and the rear boom as shown in Figures 2 and 3.

Straight Plane Design and Construction

The straight plane model was designed using the dimensions of the Bay Defender prototype (Diprofio, 1998). A straight plane model was designed using scaled dimensions and a fifteen degree angle of attack for the submergence plane.

The straight plane model was built by first constructing a set of triangle trusses to create a frame, then attaching a sheet of low-density-polyethylene (LDPE) plastic to the frame (see Figure 9 and 14). Five trusses were made of 1x2-inch nominal soft pine fastened together by drywall screws and connected together by cross-supports to create a sturdy structure. The thought was that the submergence plane should not bow under high-speeds like the full-scale prototype fabric surfaces. Interestingly, the first attempt of making a straight plane model was created using 2x4-inch nominal boards stripped in half and quarter-inch PVC plane material. This model was bulky, unwieldy and difficult to fix in the tank, requiring two people to install. The later 1x2-inch nominal models proved to be significantly lighter and equally as stiff as the 2x2-inch nominal models, making it much easier to install and remove from the flume tank.

The material selected to create the actual submergence plane was quarter-inch opaque LDPE plastic, attached to the wooden frame using drywall screws with the heads countersunk flush with the surface. (In hindsight though, a thinner PVC submergence plane would have been better, say one-eighth-inch, since it is lighter, yet just as stiff and pliable to the various submergence plane shapes.)

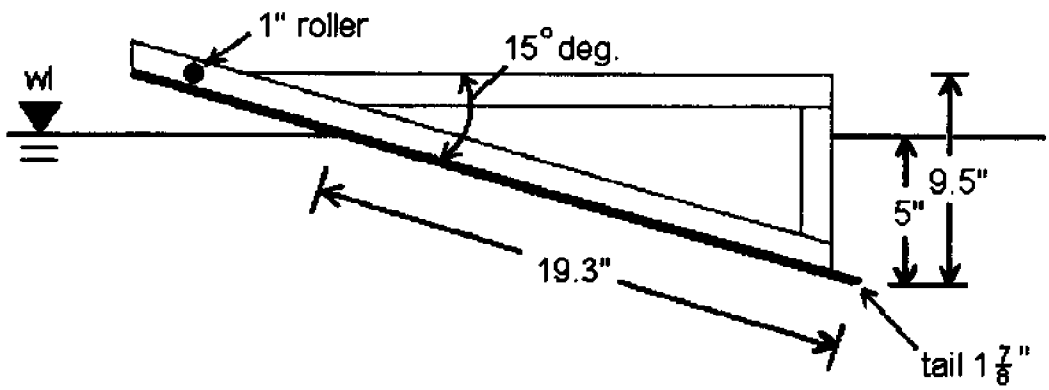

Figure 9: Straight Submergence Plane Model Dimensions

Convex Plane Design and Construction

The second submergence plane shape kept the same draft and angle of attack, but instead of having linear profile, the convex shape deflected upwards creating the arch as shown in Figure 10 (see photo in Figure15). The amount of deflection was arbitrarily chosen through a series of hand sketches on graph paper. The final curve was selected since it resembled the "cusping" shape experienced. The convex plane was formed using the following criteria; the shape remained at the five-inch draft and fifteen-degree angle-of-attack as the straight plane, but includes a deflection of one and a quarter inches perpendicular to the straight plane at four and a half inches up from the trailing edge

(refer to Figure 10 again). This shape makes the convex plane the shortest in length and smallest wetted-surface of all of the designs.

The construction of convex plane was similar method to that of the straight plane. The frame again used five trusses made of 1x2-inch nominal pine with the desired convex shape cut into a 1x8-inch nominal pine board. Cutting the desired curve in the 1x8 using a jigsaw was much simpler than trying to build the tricky curve with 1x2s. Cross-members of 1x2-inch nominal pine were again added to create the convex frame. Figure 11 shows the primary dimensions of the convex plane. The quarter-inch polyethylene sheet was then clamped to the frame with C-clamps and fixed in place with countersunk screws. The trailing edge of the plane or "tail" was not as long as with the straight plane, because the stress-relieved LDPE wanted to remain straight causing an undesirable, wavy edge on the plane.

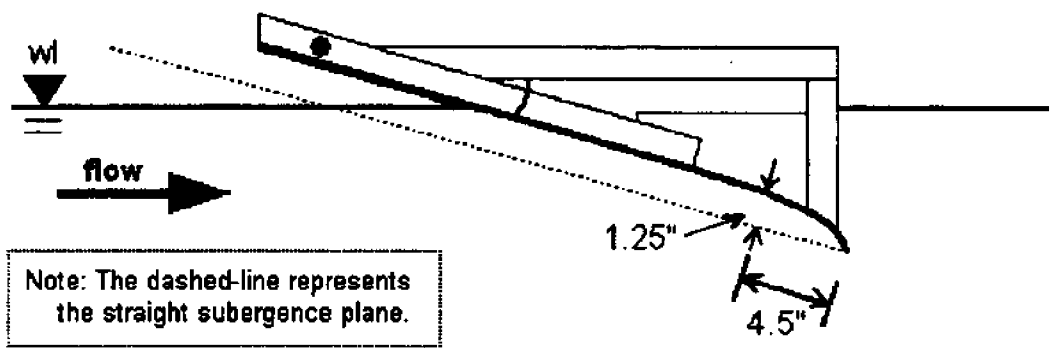

Figure 10: Convex Submergence Plane Concept

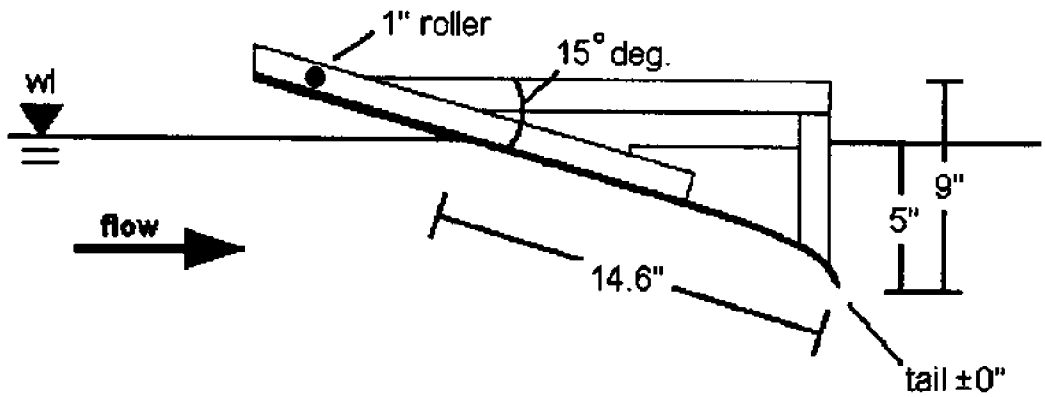

Figure 11: Convex Submergence Plane Model Dimensions

Concave ("J") Plane Design and Construction

The design of the concave submergence plane can be thought of as the exact inverse of the aforementioned convex shape. Instead of having an inward deflection like the convex plane, the concave plane bulges outward an equal amount, while maintaining the five-inch draft and fifteen-degree angle-of-attack criteria (see Figure 12 and 16). This design makes the convex shape have the largest wetted-surface of all the planes.

The construction of the concave submergence plane was similar to the methods used for the other planes. The frame was fashioned from 1x2-inch nominal boards with the 1x8-inch nominal board having the cutout of the concave shape. Once the frame was completed, the plastic sheet was fitted, clamped, and screwed into place. Figure 13 gives the primary dimensions of the concave model.

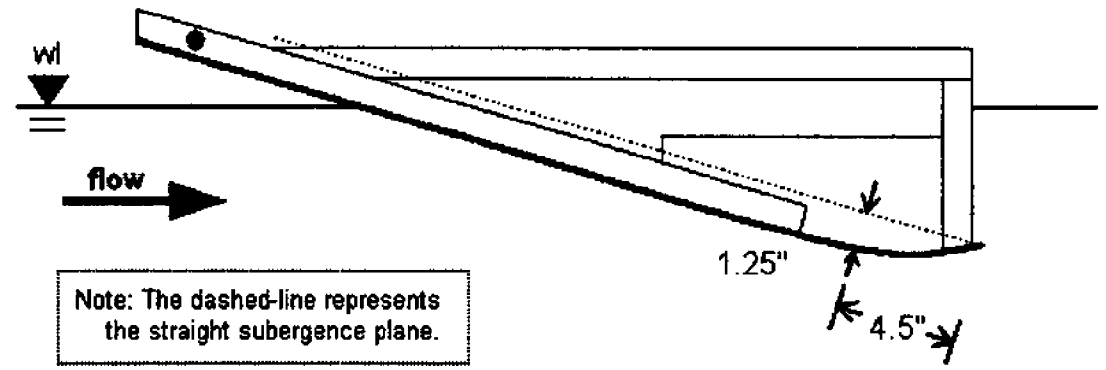

Figure 12: Concave Submergence Plane Concept

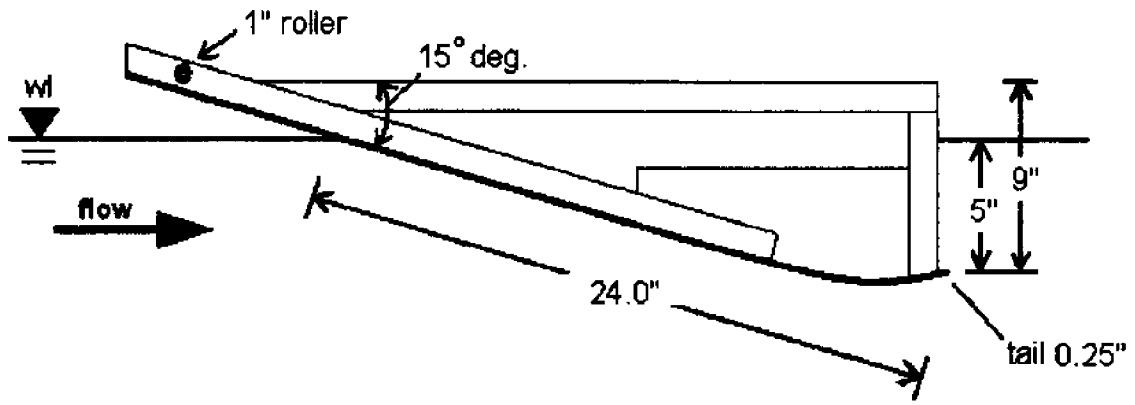

Figure 13: Concave Submergence Plane Model Dimensions

Horizontal Baffle and Rear Boom Design and Construction

The final two components of the Bay Defender prototype were the horizontal baffle and the rear boom as shown in the Figure 3 photograph. The horizontal baffle served the important functions of creating a flat barrier to eliminate entrainment failure and to allow excess water to flow out of the exit holes. The baffle fit snuggly widthwise

in the flume and had a length of forty-eight inches. This was smaller than what the scaled baffle should have been, but since space in the flume was limited, it was felt that shortening the baffle would not effect comparisons between the shapes. As shown in the results of the bead testing experiments, the length of the horizontal baffle proved to be an important factor in bead retention, such that the horizontal baffle needed to be modified.

Our original horizontal baffle was made of quarter-inch sheet of plywood treated with pool paint to prevent it from wood degradation and bending, since it would be submersed for long periods of time. Not long after being submersed in the flume, the plywood showed signs of warping. The plywood piece was replaced with a quarter-inch sheet of PVC plastic. To mount the baffle in the flume tank, wooden legs were attached to the baffle and clamped to the top of the sidewalls. By design, the area of holes in the horizontal baffle equaled the gap inlet area between the submergence plane and the horizontal baffle. These holes were created using a two-and-three-eighths inch hole saw.

The rear boom, which was needed to close off the back of the containment system, consisted of a vertical PVC barrier. The boom was set to match the draft of the horizontal baffle. Supports were added to the barrier to fix the baffle firmly to the flume's sidewalls. The position of the rear boom was approximately 7.16 inches back from the end of the horizontal baffle. This value was chosen, since it equaled the inlet area (distance from the tail of the submergence plane to the front of the baffle using the Pythagorean theorem). By design, the exit area created by the horizontal baffle and rear boom equals the exit area of the baffle's holes. When these areas are added together, they equal twice the inlet area. This allows for adequate exiting flow for any excess water in the containment region.

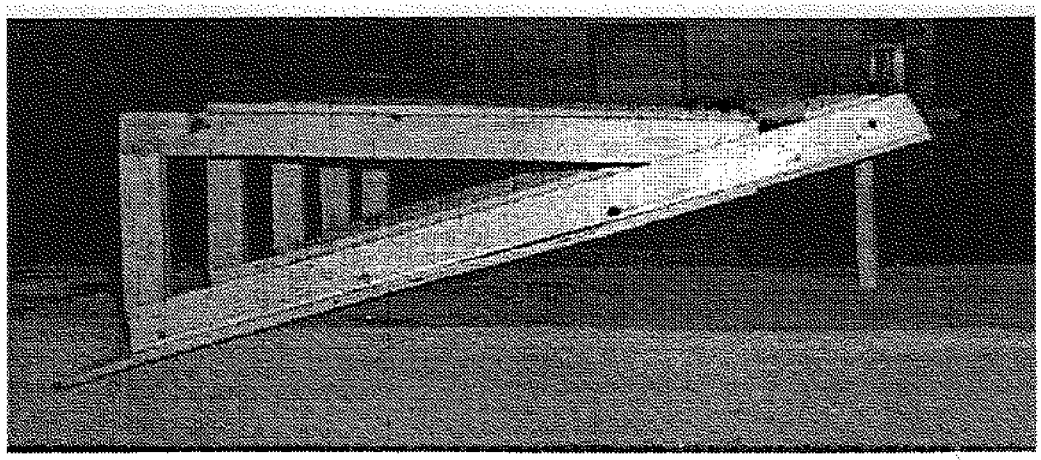

Figure 14: Photo of the Straight Submergence Plane Model

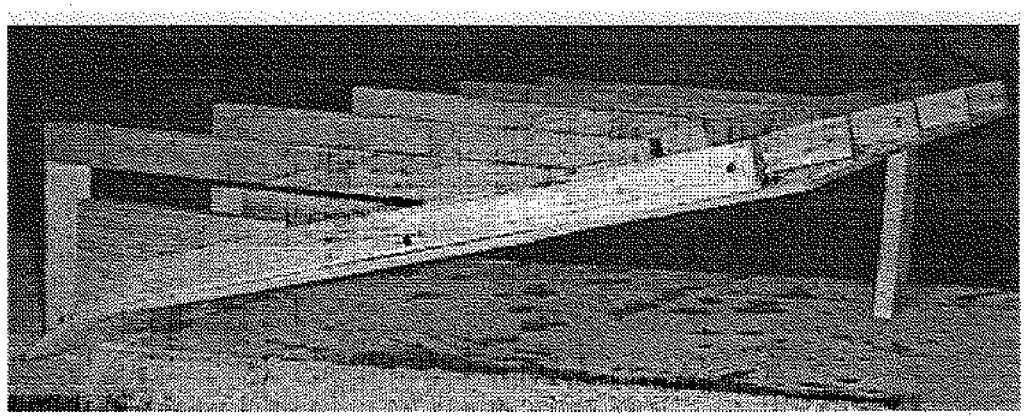

Figure 15: Photo of the Convex Submergence Plane Model

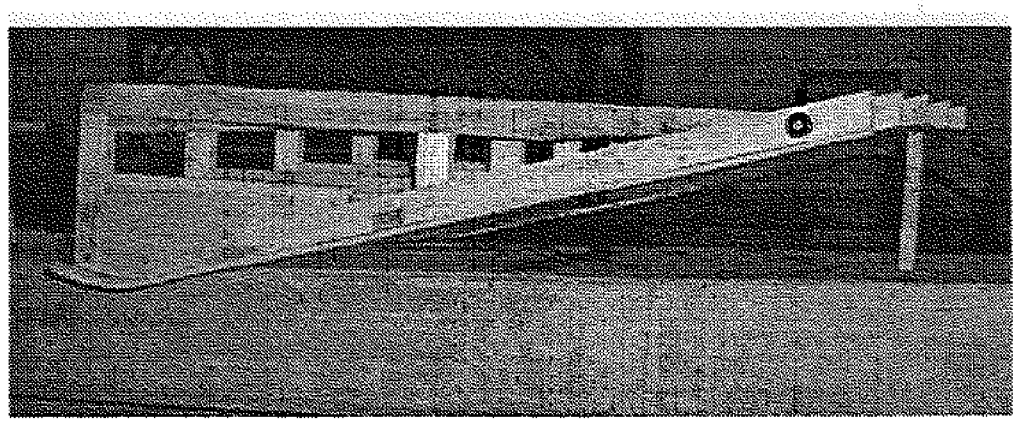

Figure 16: Photo of the Concave Submergence Plane Model

CHAPTER 4

Testing and Results

Flume Calibration

As mentioned in the Testing Facilities section, the flume tank is controlled by entering the input motor frequencies of the frequency driver, which in, turn powers the dual electric motors. Previous work had been done to calibrate the flow speed expected for a known input frequency, but since an electromagnetic flow meter was available, the flume was recalibrated with the complete scale models in place. This would insure that flow would be consistent with actual test conditions when the submergence plane, horizontal baffle, and rear boom were mounted in the flume. It was assumed that with these structures in place, some resistance would be added to the flow, thus slowing the incident velocity of the water in the flume. The calibration tests were performed in the center of the tank, eighteen inches in front of the submergence plane to ensure that the stagnation area would not effect the velocity readings. These tests were performed at varying depths as well as across the flume's width to insure that the flow did not deviate greatly due to location.

Flow measurements for the flume calibration were performed using the Marsh-McBirney Flo-Mate 2000 flow meter. The Flo-Mate 2000 operates by emitting a magnetic field, so as a conductor, i.e. particles of water, pass through the field a change in voltage is produced. This change in voltage is directly proportional to the velocity of the conductor passing through. A more detailed theory on how the Flo-Mate 2000 flow meter operates refer to Appendix A.

The configuration for the flume calibration setup, similar to other tests, was arranged as described below (refer to Figure 5 for terminology). The straight submergence plane was held rigidly in place with five inches of draft. The horizontal baffle was positioned with a draft of six-and-quarter inches (therefore, a "bite" of one inch) and seven inches behind the submergence plane. Following the horizontal baffle, the rear boom was installed in place, just over seven inches behind the baffle.

Calibration measurements ran from a motor frequency of zero to fifty Hertz at intervals of two-and-a-half Hertz. Each flow meter reading recorded was taken over an averaging period of at least sixty seconds. This was necessary, due to the precision of the flow meter and the fluctuation of the fluid flow. Tests began in the center of the tank with the flow meter three inches below the water's surface for a series of three tests, then it was lowered to depths of five and six inches, respectively. Following the measurement taken in the center, the flow meter was moved to halfway between the center of the tank and the wall. The same procedure was performed at depths of three and six inches. Raw data from the calibration tests can be found in Appendix A.

Results for the calibration tests show that over a range of input frequencies, the flow velocity in the center of the flume remains relatively constant as the depth increases. Flow measurements taken off center of the flume show that the flow was typically a few tenths of a foot per second faster than those recorded in the center. This is thought to be associated with the position of the propellers in the flume. The variation in flow speeds was disregarded as an insignificant source of error. The data obtained from the center position was used for our flume calibration for the test-section.

Figure 17 shows a graph of five test averages for the flume calibration. A linear-fit was then added to the graph to show the linearity of the flow velocity in the test-section verses the input frequency. Table 3 in Appendix A has the calibration data in an easy-to-read tabular form. For a given input frequency, the conversion table shows what

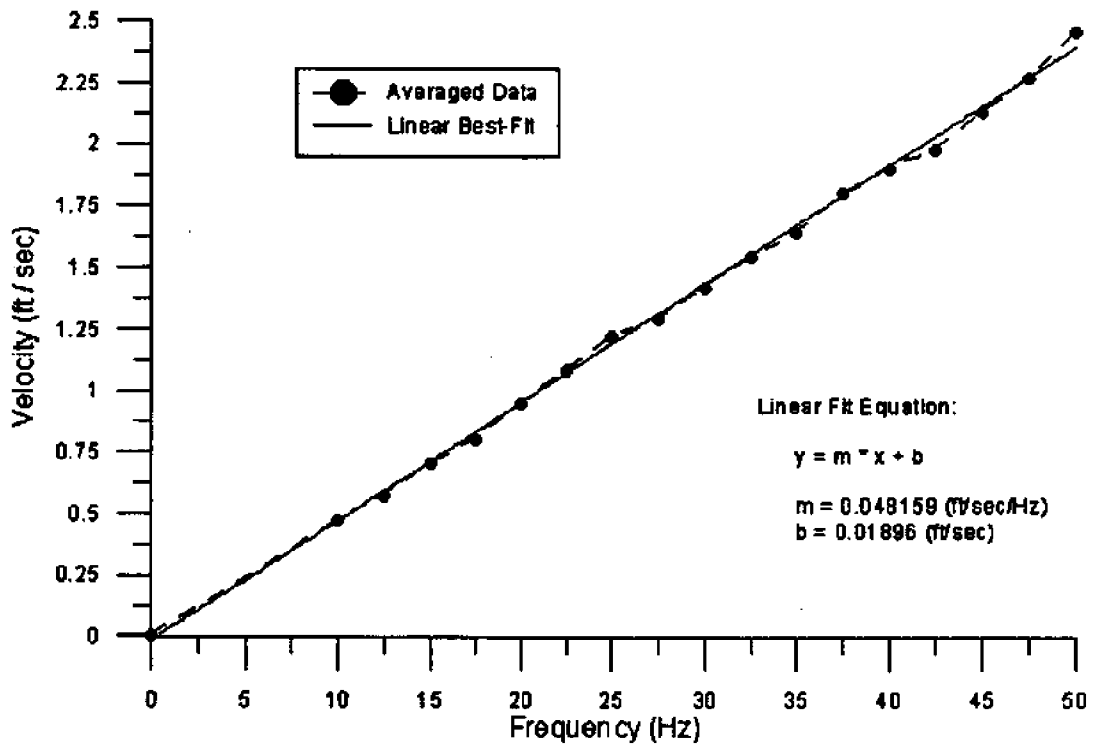

Figure 17: Calibration Graph

flow speed one can expect. Changes in speed are not instantaneous; roughly one minute is required between frequency changes to ensure the flow is up-to speed and fairly uniform.

Lift and Drag Test Methodology

The lift and drag forces of the various submergence plane shapes were determined through the use of a ten-pound load cell. The determination for the size of load cell needed was done through a conservation of mass and momentum control volume analysis. A Mathcad worksheet of the theoretical calculations can be found in Appendix B. Fortunately, the load cell used was acquired through a previous study conducted in the flume tank. This happened to save the project a significant amount of money (see Chapter 5, Budget and Finances).

In the construction of the submergence planes, each plane was fitted with a steel wheel located at the front of the planes. (Figure 18 has a photo of the steel roller assembly) The wheel was connected to the submergence plane simply with a steel bolt, which had been greased to keep the frictional effects at a minimum. Once the submergence plane was installed in the flume, the wheel would slide into a wooden track, roughly eight inches in length, which was mounted to each side of the flume (as in Figure 18). The track would allow the submergence plane to pivot about its wheel, as well as give freedom of movement in the horizontal direction. The width of the track was one inch, so that the roller of equal size could not move vertically in the track. Figure 18 shows a photograph of the track and roller setup.

Figure 18: Photo of the Track and Roller Setup

Next, a section of light static line was connected at the pivot points of the submergence plane and attached to the load cell, shown in Figure 19. The load cell was mounted horizontally inline with the pivoting points, roughly three feet in front of the submergence plane. It was also important for the lift and drag experiments that the LDPE sheets on the planes were cut as wide as possible, yet did not rub against the walls of the flume, as this would effect the load cell's accuracy.

Figure 19: Photo of the Load Cell Setup

A detailed procedure for the lift and drag experiments is outlined by the Lift and Drag Testing Protocol found in Appendix B. Raw data from the sixteen lift and drag tests can also be found in Appendix B. The straight and convex submergence planes had three sets of lift and drag tests used in analysis, while the concave submergence plane had two sets of lift and drag tests. An average was taken for each of the lift and drag tests used. A number of the earlier tests were discarded after the horizontal boom was changed from plywood to PVC and a change was made to the size of the exit area between the horizontal baffle and rear boom. These changes affected the lift and drag experiments and therefore were not used in the analysis. It was important to keep everything consistent for all tests.

Using the load cell measurements and the amount of weight added, the lift and drag forces acting on the plane could be found through summing the forces and moments acting on the submergence plane. Since the solution of these equations relied only on the load cell reading, a few assumptions needed to be made concerning the lift and drag results:

1) High accuracy of load cell reading
2) Negligible frictional effects in the steel rollers
3) Resultant force (P) acts normal to the submergence plane

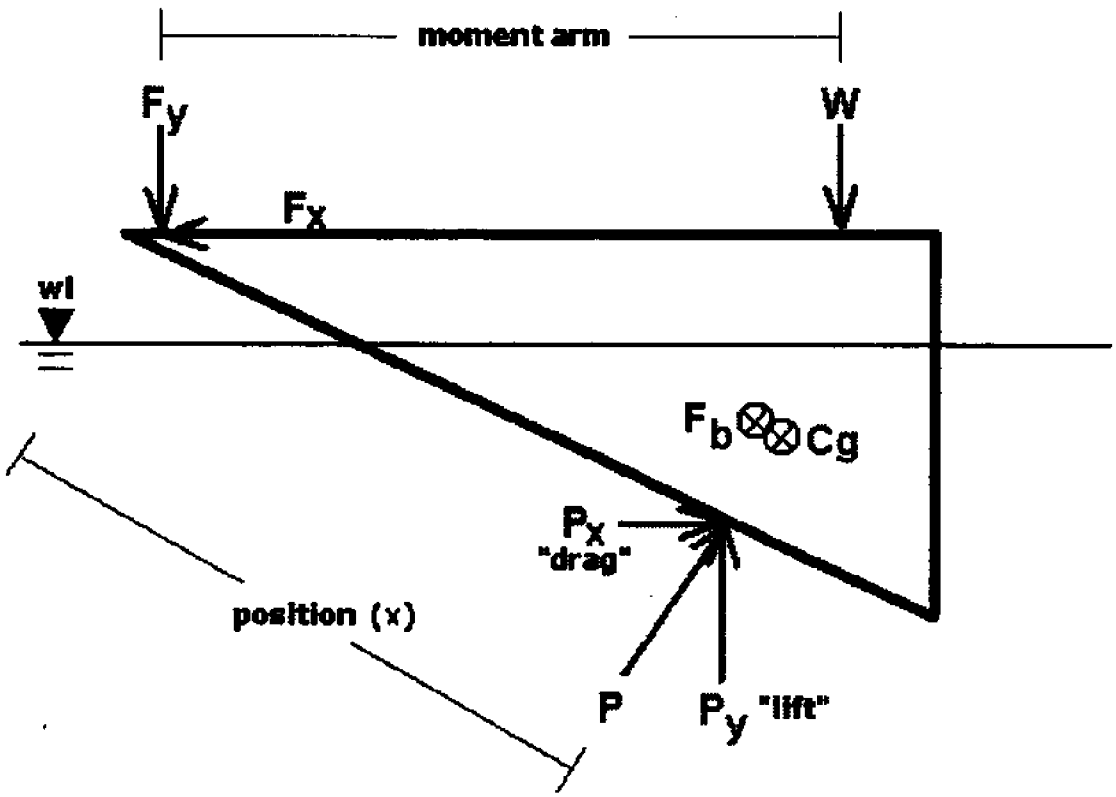

Figure 20: A Free-Body Diagram of the Submergence Plane

The free-body diagram in Figure 20 shows the forces acting on the submergence planes at equilibrium.

Lift and Drag Results

The results for the lift and drag section were compiled into a graphical form to better visualize the data and its patterns. Figures 21, 22 and 23 show the lift and drag results for the straight, convex and concave plane, respectively, while Figure 24 compares the drag forces for all of the submergence plane shapes. The comparative analysis was performed simply using the drag forces from the load cell, since the other forces were determined using the drag force.

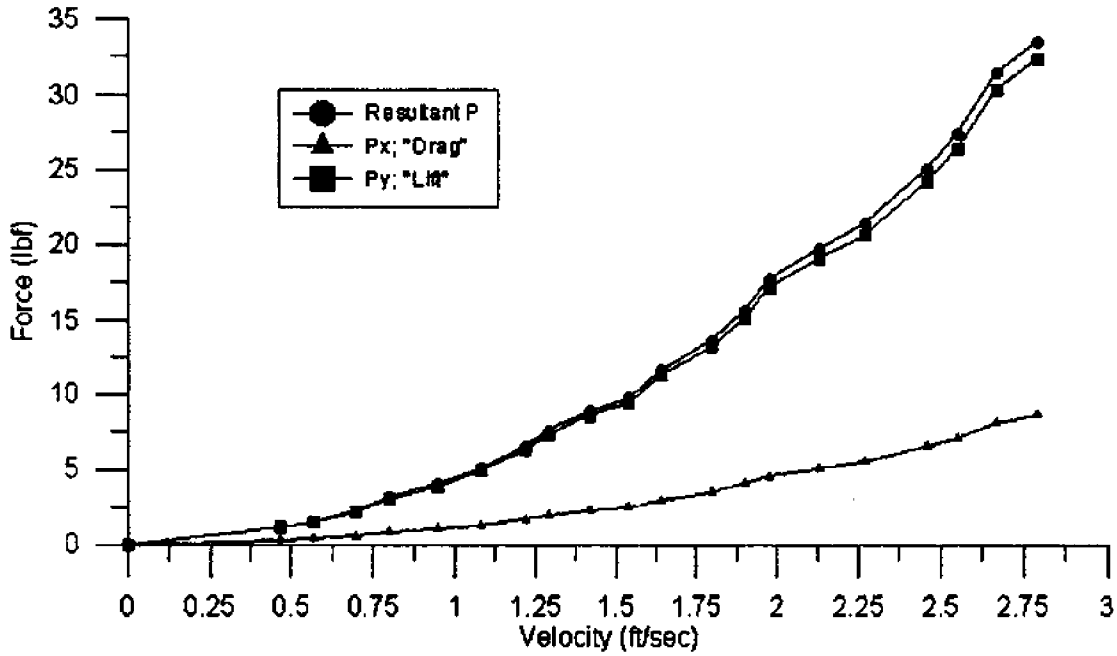

Figure 21: Graph of Lift and Drag Forces for the Straight Submergence Plane

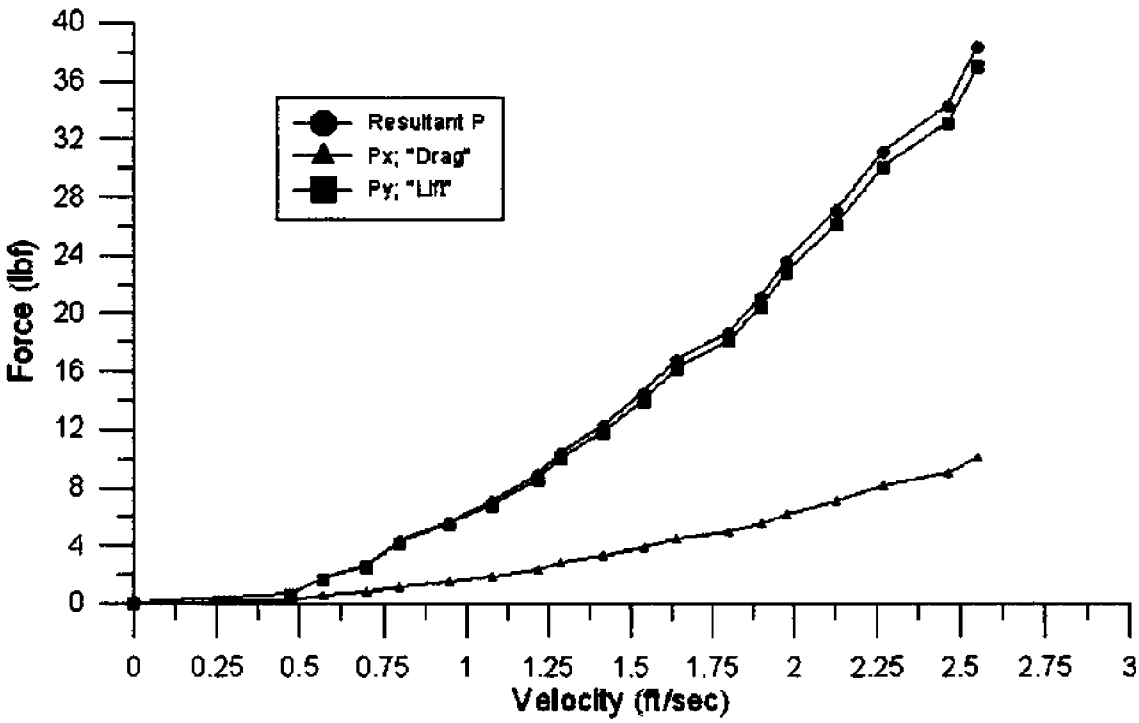

Figure 22: Graph of Lift and Drag Forces for the Convex Submergence Plane

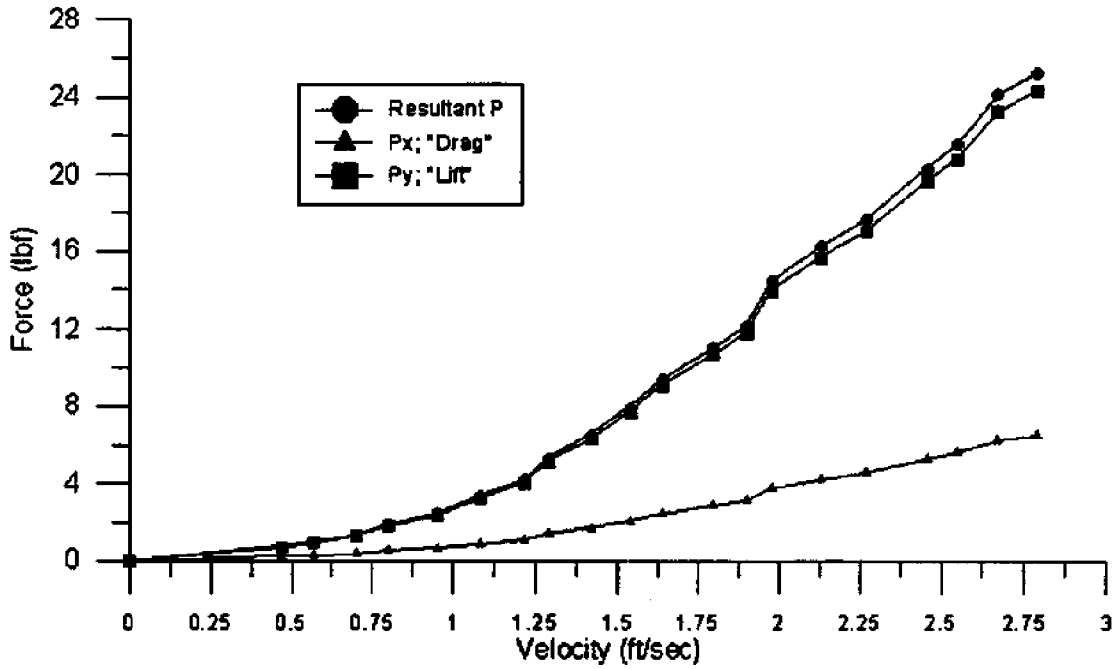

Figure 23: Graph of Lift and Drag Forces for the Concave Submergence Plane

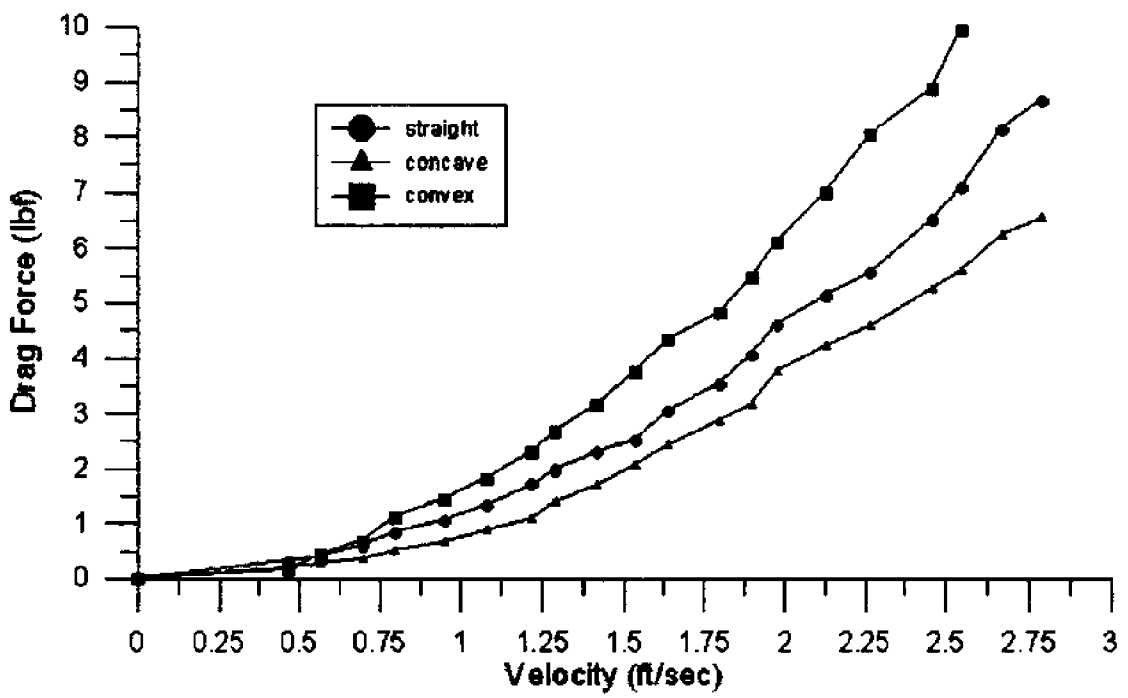

Figure 24: Graph of Drag Forces for all Three Plane Shapes

From a simple glance at the graphs, one can clearly see that the convex submergence plane induces the most amount of drag, while the concave plane creates the least. This was obvious through the testing as well, since the convex plane required the most amount of added weight in order to keep the draft at the five-inch draft line. The straight plane took a fair amount of weight in order to keep it in position, but clearly the concave plane needed the least amount of weight. Through calculations over the range of flow velocities, it can be shown that the convex submergence plane produces on average 38.3 percent more drag than the straight plane. Conversely, the concave plane reduces the amount of drag by an average of 24.4 percent compared to the straight plane.

The convex submergence plane had an undesirable lifting effect at the high ranges of speed, while the concave plane distinctly performed the lift and drag experiments as hoped, having the lowest lift and drag results of the three models. Through knowing these lift and drag forces on the scale models, it is intended that future submergence plane designers can use the data to aid in future Bay Defender designs.

Flow Measurements

Flow measurements inside the containment region were recorded at four different locations using the Marsh-McBirney Flo-Mate 2000 flow meter. Figure 25 shows a schematic of the locations where the four flow measurements occurred. Two of these

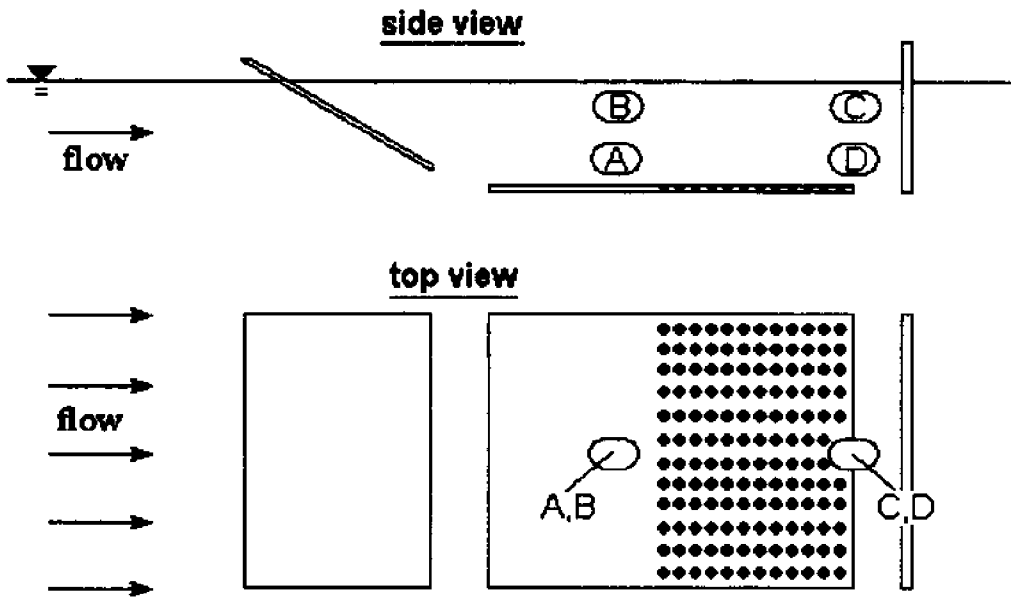

Figure 25: Diagram of Positions Tested using the Electromagnetic Flow Meter

measurements were taken fifteen inches back from the front edge of the horizontal baffle, just in front of the exit holes. At this position, an upper (B) and lower (A) set of measurements was recorded. The upper reading was taken at a depth of two inches below the water's surface and the lower was four-and-a-half inches below the surface. The third and fourth set of measurements were recorded directly above the trailing edge of the submergence plane, forty-eight inches from the front end of the baffle. Once again this position had a set of upper (C) and lower (D) readings at the same aforementioned depths.

The initial flow meter measurements were completed at position A using the straight submergence plane with a bite of one inch. Early testing showed that a minimal amount of flow entered the containment area, even with an input frequency of forty Hertz, approximately 1.9 feet per second. Similar results were obtained at the other designated testing locations. A unanimous decision was made to increase the amount of bite to one-and-a-half inches by lowering the horizontal baffle half-an-inch. This remained constant throughout all the flow measurements and for the bead testing. All other inlet and exit gap geometries remained the same as discussed in Chapter 2.

The procedure for recording flow measurements stayed consistent to the methods for flume calibration. An average velocity was determined over a period of at least sixty seconds. Multiple sets of measurements were taken at each location (A, B, C, or D), with the exception of places where it was deemed unnecessary because of the amount of turbulence. Areas of strong intermittence gave random flow velocities, where the flow would occasionally be positive, other times negative. These readings were valueless and full of error. All tests performed began with an input frequency of ten Hertz and finished at 52.5 Hertz with increments of 2.5 Hertz.

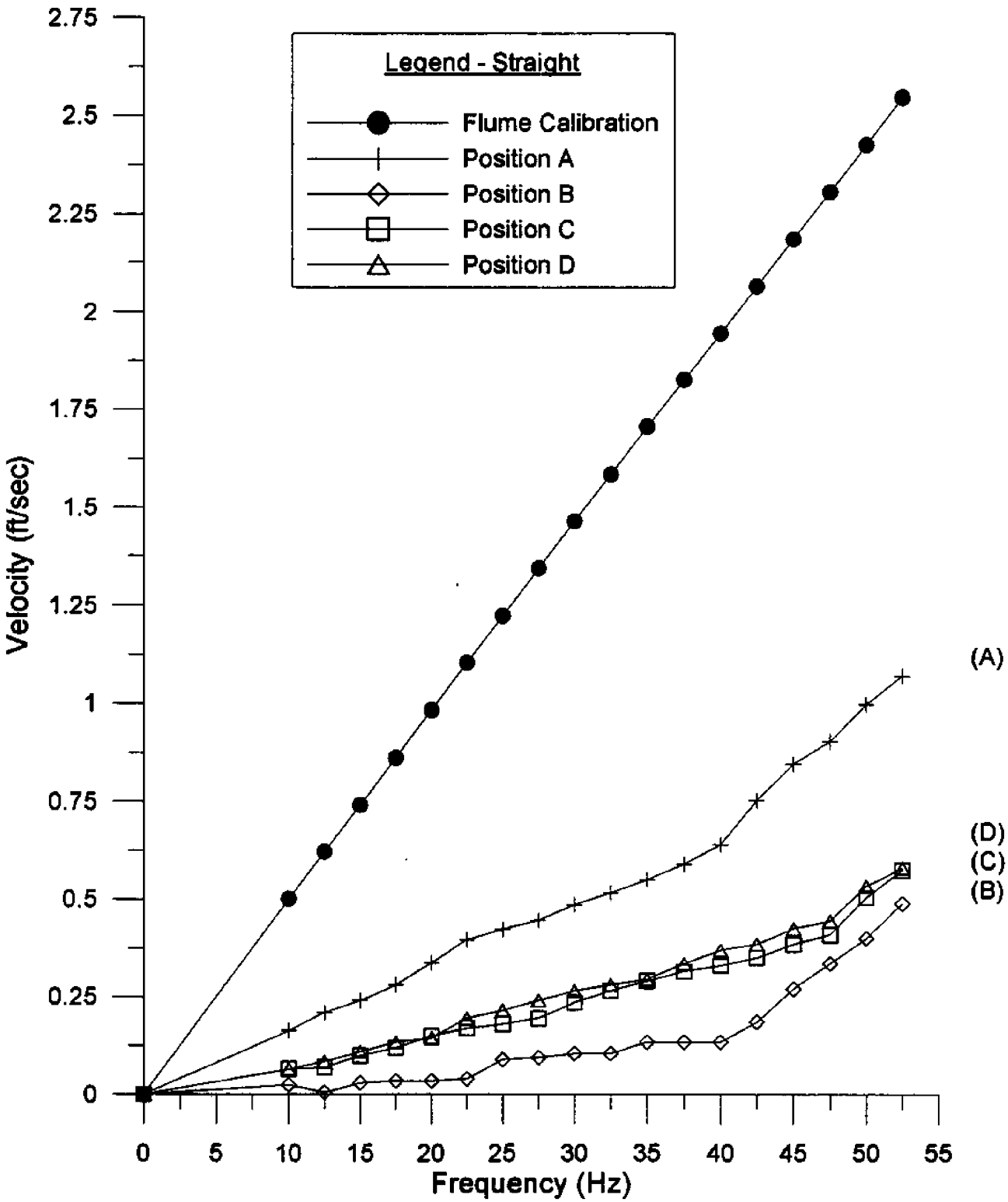

Figure 26: Graph of Straight Plane Flow Measurements

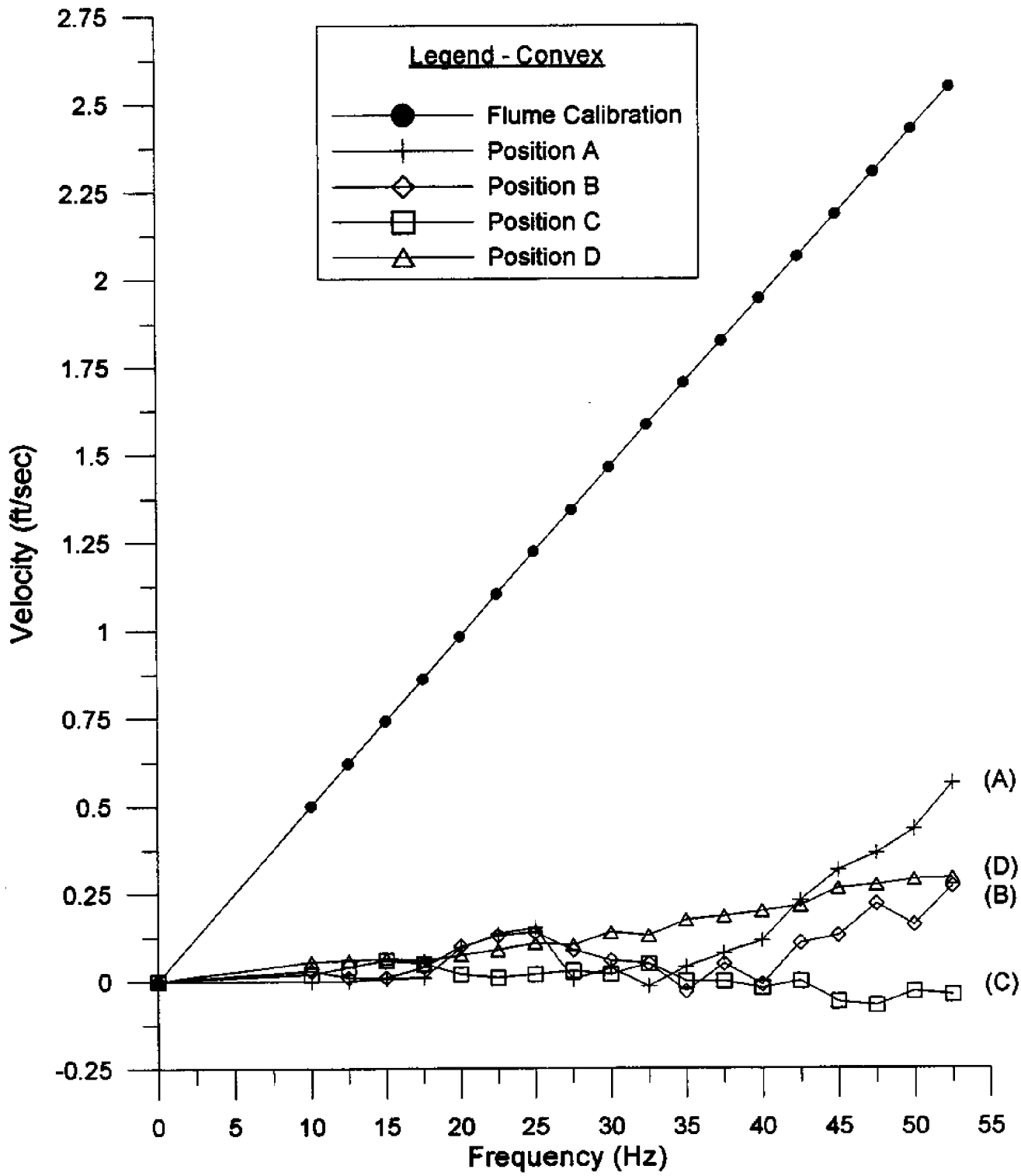

Figure 27: Graph of the Convex Plane Flow Measurements

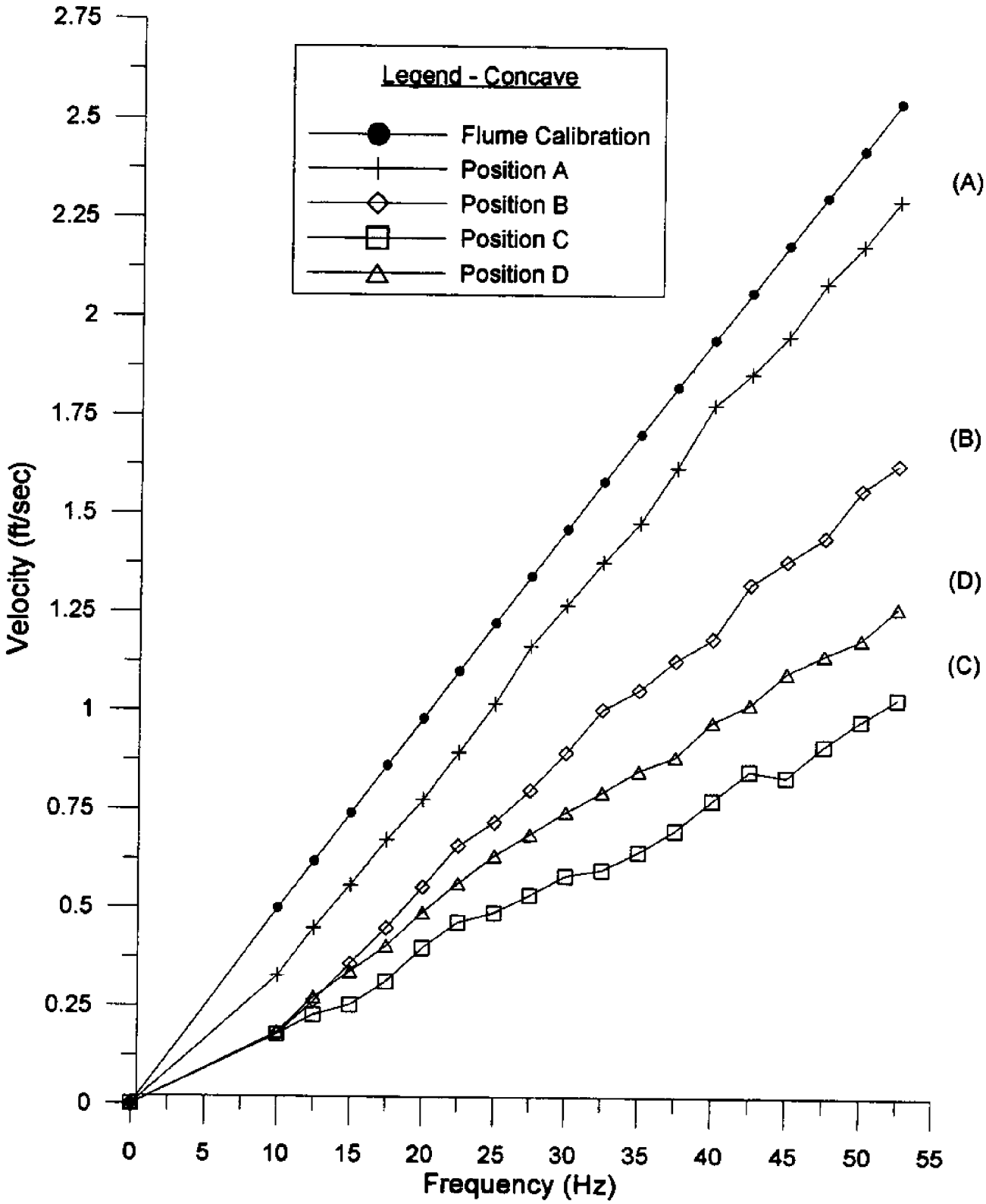

Figure 28: Graph of the Concave Flow Measurements

Results from the flow measurements inside the containment region are shown in graphical form in Figures 26 through 28. Refer to Figure 25, as needed, for a drawing of the labeled test positions.

Figure 26, the graph of the straight submergence plane, suggests that most of the flow enters through Position A, which is to be expected. Positions D shows that much of the containment flow exits through the gap instead of the holes in the baffle. Position C appears to have less flow than position D. Position B suggests that the flow is fairly stagnant, which is a good result, since this is where the contained oil remains.

The results of the convex submergence plane in Figure 27 prove that much of the flow misses the inlet area and containment region. At low motor frequencies below forty Hertz, there is little to no water movement at any of the four positions. Much of the flow is essentially zero, fluctuating between positive (forward) and negative (backward) flow. Above forty Hertz, positions A, B and D produce positive flow, yet nothing of strong magnitudes. Position C at the top of the exit area, remains still.

Figure 28 shows the results of the flow measurements for the concave plane. Here much of the flow turns the corner and shoots into the containment region. Position A has the greatest amount of flow, just slightly less than the incident flow for the test-section. Position B also has strong positive flow suggesting the flow rises as to just below the water's surface. As the water moves backwards, much of it exits through position D, leaving position C with the least amount of water movement. There is a drastic difference in the movement of water in the containment regions of the concave and convex submergence planes. Even though the concave plane seems to direct the flow

into the containment region, too much flow inside can have adverse effects. It would be beneficial for future studies to determine the ideal amount of "bite", allowing the flow of contaminants through the inlet without the excess flow of water.

Bead Testing Methodology

Bead testing experiments allow for good comparative studies and are an alternative to using actual oil experiments avoiding the hazardous handling and messy cleanup. Despite the ease of bead cleanup compared to oil, each bead test required many hours of time to clean out every nook and cranny of the flume tank. On top of that, it was necessary to have at least five people to run the bead test, so naturally, the logistics of timing were difficult. All seven bead tests were performed at a current speed of one-and-a-half knots. Of these seven tests, only six were used for comparative analysis. Two tests were conducted for each of the three submergence plane designs to ensure some consistency in the amount of beads retained. More tests should have been conducted had time permitted, to observe the consistency of the results through statistical analysis.

The physical configuration of the model components for bead testing experiments was identical to those during the previous flow measurements. The horizontal baffle was placed seven inches back from the submergence plane with a bite of an inch-and-a-half. The rear boom had the same draft as the horizontal baffle and had an exit length of 7.16 inches. Two items differed during bead testing than during the other experiments. One difference was that the edges of the submergence plane against the sidewalls were sealed

off using an adhesive foam. This prevented beads from slipping in along the sides. The second difference was that a fine mesh screen was installed the baffle and rear boom to prevent beads from escaping out the back end of the baffle. This was witnessed days prior to the formal bead testing experiments. The addition of the screen was deemed necessary in determining the actual containment of the submergence planes. Since the project focused comparative studies of the submergence planes, the addition of the screen had no significant effect on the retention percentages.

A brief procedure of the bead tests is outlined below, but for a more detailed procedure refer to the Bead Testing Protocol found in Appendix C. Since the tests were performed for comparative purposes, it was vital for each test to be conducted in the same manner.

Briefly each test was performed by releasing three liters of small plastic beads via a hopper into the flume tank, just past the flow straighteners. The plastic beads used had a similar specific gravity to oil, so they mimicked actual oil tests well. Ideally, the beads once poured would remain on the surface of the water as they traveled down to the submergence plane (although it was seen that many of the beads would sink sub-surface from the pour, thus missing containment). Once all of the beads had encountered the system, the motors were cut abruptly and the flow was allowed to settle. Since the momentum of the water at a knot and a half is so great, a good amount of time passed before the flow came to a stop. After being deployed into the flume, the beads would either enter the containment region or would cycle around through the propellers for a second pass. This second chance was undesirable, since they would alter the actual percentages of beads retained.

Once everything came to a stop, the beads were collected first from the containment region, then the rest were recovered and placed in separate containers. This was the part which was so time-consuming. After being collected and stored, the beads were allowed to dry overnight before being volumetrically measured. Containment percentages were determined by dividing the volume retained by the volume of beads introduced. Bead testing results are in tabular form in Table 1.

Bead Testing Results

Test #	Submergence Plane Shape	Bead Specific Gravity	Volume Introduced	Volume Contained	Volume Lost	Retention Percentage
practice	Straight	0.89	3000 ml	2900 ml	100 ml	96.7 %
1	Straight	0.96	3000 ml	2620 ml	380 ml	87.3 %
2	Straight	0.96	3000 ml	2550 ml	450 ml	85.0 %
3	Convex	0.96	3000 ml	1450 ml	1550 ml	48.3 %
4	Convex	0.96	3000 ml	1330 ml	1670 ml	44.3 %
5	Concave	0.96	3000 ml	2420 ml	580 ml	80.7 %
6	Concave	0.96	3000 ml	2350 ml	650 ml	78.3 %

Table 1: Summary of Bead Testing Results

The initial bead test performed was labeled a practice because of the number of beads, which had a "second chance", and the specific gravity of the beads was changed. Changing the bead's specific gravity was done to show a greater difference between the straight submergence plane and the concave submergence plane, which was thought to have the best retention capability. The remaining bead tests performed used beads with a specific gravity of 0.96, which resembled Sundex oil.

The straight submergence plane tests resulted in an average of 86 % bead retention. Eighty-six percent is considered a fair result, though it certainly could be bettered. A certain amount of the "lost" beads can be attributed to the dumping method, as many sunk below the surface, never having a chance to encounter the submergence plane. On the other hand, no matter what was done to prevent it, some of the lost beads had a second chance for containment.

Bead tests conducted on the convex submergence plane gave expected results as previously theorized. Less than half of the beads, forty-six percent on average, were contained for the convex shape. Observations during testing suggest that the majority of beads followed the flow of water and shot past the inlet area. If the "Bay Defender" cusps, as mentioned in Chapter 1, oil containment will be impaired at speeds near or greater than a knot and a half.

The concave submergence plane had the most surprising results of all the planes. Throughout the project, it was assumed this plane would have the highest retention percentages, but it averaged eighty percent containment, six percent lower than the straight plane.

Despite these results, it is still felt that the concave plane shows promising signs of improving oil containment in fast-moving currents. Had time permitted, two changes in the bead testing experiments would have been carried through. First, the method of bead dumping could greatly be improved by making the pour more uniform and preventing the beads from sinking below the water's surface. The second change would be to build a fine-mesh screen to span the cross-section of the flume, in order to function

as a barrier preventing lost beads from a "second chance" of containment. The screen would be set in place in front of the submergence plane directly following the bead slick.

CHAPTER 5

BUDGET AND FINANCES

Of the money allotted for the S.P.A.M. project, only half of the budget was spent at the end of the project in April. The building materials and tools needed for the construction of the three models totaled $400.19. This money was primarily spent on wood for the frames, numerous C-clamps, and the low-density-polyethylene sheets needed for the plane material. The ten-pound load cell used for the lift and drag experiments was acquired through a previous engineering project, thus saving the project nearly three hundred dollars. The Marsh-McBirney Flo-Mate 2000 was the largest expenditure for the project. Nearly six hundred and twenty dollars was spent towards purchasing the flow meter, yet this was a fraction of what the unit cost, since it was a collaborative investment between many projects. The flow meter will be a handy device for many future Ocean Engineering projects. The total amount spent on testing supplies was $647.58. Finally, twenty-two dollars was spent on presentation materials, such as photographs and paper supplies.

The total amount spent on the submergence plane project was $1069.66 of the $1975.00 allotted budget. An itemized list of expenditures is provided in Table 2 on the following page.

Budget and Finances

		total cost
Construction Materials:		
1x2s		$64.14
2x4s		$35.15
plywood		$15.74
LDPE sheets		$164.60
drywall screws		$13.90
bolts, washers, nuts		$7.96
C-clamps		$37.40
Thompson's Waterseal		$12.43
paint		$6.09
brush		
countersink		$8.99
duct tape		$9.98
drill dits		$12.99
drill heads		$6.79
jigsaw blades		$3.98
	Construction Total	$400.14
Testing Supplies:		
Marsh-McBirney Flo-Mate 2000		$619.35
D-cell batteries		$5.59
screen		$2.58
Fish nets		$20.06
	Testing Supply Total	$647.58
Presentation Materials:		
photos		$12.00
video tape		$2.99
paper		$6.95
	Presentation Total	$21.94
	Total SPAM Budget	$1,069.66
	Budgeted	$1,975.00
	SPAM saved	$905.34

Table 2: Itemized List of Expenditures

CHAPTER 6

Conclusion and Further Study

The goal of the project in its entirety was to observe how the shape of the submergence plane affects the lift and drag forces, the flow through the containment region and finally, the bead retention characteristics. Ideally, the goal of this study was to see how the change in submergence plane shape may improve todays prototype's ability to contain oil at greater current speeds than what is currently possible. The submergence plane devices, thus far, have shown to be an improvement over conventional oil booms, nearly tripling the critical failure velocity of a vertical barrier. The three submergence plane shapes tested clearly prove that the shape of the inclined surfaces affect the performance of the oil containing devices.

Through the lift and drag experiments, it is clear that changing the submergence plane shape will alter the dynamic lifting effects for the entire device. By changing the plane design to a concave shape, the lifting forces could be reduced by nearly twenty-five percent, thus not effecting the gap geometries between the submergence plane and the horizontal baffle as severely. The convex submergence plane resulted in the largest lifting and drag forces, so it is obvious that if the fabric material of the "Bay Defender" cusps in this shape, negative results can be expected.

The series of flow measurement readings show that the change in submergence plane shape greatly affects the amount of flow in the containment region, despite the inch-and-a-half bite between the plane and the baffle. The convex plane shoots the flow of water past the inlet area, causing the containment region to be very still or stagnant.

The straight plane does allow flow into the containment region, but the majority of it stays low hugging the horizontal baffle. The concave plane, on the other hand, redirects the flow into the containment region, which can have both positive and negative effects on oil containment; positive, because all of the oil travelling down the submergence plane will enter through the inlet area, but negative because the amount of flow into the system must exit, possibly taking some of the contained oil with it.

Bead tests conducted remain quite inconclusive. The convex submergence plane certainly proved that, having lost more than half of the contaminants, it is not the proper shape for Sundex oil at a knot-and-a-half. Surprisingly, the straight submergence plane collected the plastic beads better than the concave plane by roughly six percent. Further study should be conducted, however, to see whether this is an accurate result or a fallacy of the test methods performed.

From these tests, it can be concluded that the shape of the submergence plane strongly affects the possibility of collecting oil at current speeds of one-and-a-half knots or greater. Changing the submergence plane shape to a concave design has many benefits over a straight plane, although it may prove to be difficult to manufacture and transport. Further study is certainly required to determine the ideal submergence plane shape and to outweigh the benefits and disadvantages of creating a more complicated submergence plane curve.

REFERENCES

1) Agrawal, R.K. and L.A. Hale, (1974) "A New Criterion for Predicting Headwave Instability of an Oil Slick Retained by a Barrier", Proc. of the Offshore Technology Conference

2) Bianchi, R.A. and G. Henry, (1973) "The Development and Demonstration of an Underwater Oil Harvester Technique", Report submitted to the EPA

3) Coyne, Phillip M., (1995) "Development of a Fast Current Oil Containment Barrier", Report submitted for Master's Thesis University of New Hampshire

4) Delvigne, G.A.L., (1989) "Barrier Failure by Critical Accumulation of Viscous Oil", Proc. of the 1989 Oil Spill Conf., American Petroleum Institute, pg 143-148

5) Diprofio, William Michael, (1998) "A Flexible, Commercial Barrier for Oil Containment in Estuaries", Report submitted for Master's Thesis University of New Hampshire

6) Milgram, J.H. and R. Van Houghton, (1978) "Mechanics of a Restrained Layer of Floating Oil above a Water Current", J. Hydronautics, Vol. 12, No. 3, pg 93-108

7) Wicks, M., III (1969) "Fluid Dynamics of Floating Oil Containment by Mechanical Barriers in the Presence of Water Currents", Proceedings API/FWPCA Joint Conference on the Prevention and Control of Oil Spills, 55-106.

APPENDICIES:

Appendix A: Flume Calibration

Appendix B: Lift and Drag Experiments

Appendix C: Bead Testing

Appendix A:

Flume Calibration

Theory of Flo-Mate Operation

The following was taken from the owner's manual of the electromagnetic flow meter, Flo-Mate 2000, made by Marsh-McBirney Inc.:

"The Flo-Mate measures flow using the Faraday law of electromagnetic induction. This law states that as a conductor moves through a magnetic field, a voltage is produced. The magnitude of this voltage is directly proportional to the velocity at which the conductor moves through the magnetic field.

When the flow approaches the sensor from directly in front, then the direction of the flow, the magnetic field, and the sensed voltage are mutually perpendicular to each other. Hence, the voltage output will represent the velocity of the flow at the electrodes.

The sensor is equipped with a electromagnetic coil that produces the magnetic field. A pair of carbon electrodes measure the voltage produced by the velocity of the conductor, which in this case is the flowing liquid. The measured voltage is processed by the electronics and output as a linear measurement of velocity.

Flowmeter Readings for Calibration

tested on: Mar 30th

tested 18" in front of straight plane
(in front of stagnation area)_

Depth 1= 3 in
Depth 2= 5 in
Depth 3= 6 in

	Frequency (Hz)	Velocity 1 (ft/sec)	Velocity 2 (ft/sec)	Velocity 3 (ft/sec)	Average Velocity (ft/sec)	Average Velocity (ft/sec)
	0	0	0	0	0	0
	10	0.47	0.48	0.46	0.47	0.47
	12.5	0.6	0.55	0.56	0.57	0.57
	15	0.74	0.7	0.65	0.696667	0.7
	17.5	0.86	0.78	0.75	0.796667	0.8
	20	0.98	0.94	0.93	0.95	0.95
	22.5	1.11	1.09	1.04	1.08	1.08
	25	1.23	1.24	1.18	1.216667	1.22
	27.5	1.25	1.33	1.29	1.29	1.29
	30	1.42	1.45	1.39	1.42	1.42
	32.5	1.53	1.5	1.58	1.536667	1.54
	35	1.66	1.64	1.61	1.636667	1.64
	37.5	1.85	1.81	1.75	1.803333	1.8
	40	1.92	1.84	1.94	1.9	1.9
	42.5	2.09	1.93	1.91	1.976667	1.98
	45	2.19	2.09	2.1	2.126667	2.13
	47.5	2.38	2.17	2.27	2.273333	2.27
	50	2.51	2.45	2.41	2.456667	2.46
*from Best Linear Fit; see Graph	52.5				2.547308	2.55
	55				2.667705	2.67
	57.5				2.788103	2.79
	60				2.9085	2.91

Expected Flow Velocity in the Flume's Test-Section

Hertz	ft / sec	knots	m / sec	mph
0	0	0	0	0
5	0.2598	0.154	0.0792	0.1771
10	0.5006	0.297	0.1526	0.3413
12.5	0.6209	0.368	0.1893	0.4234
15	0.7413	0.439	0.226	0.5055
17.5	0.8617	0.511	0.2627	0.5876
20	0.9821	0.582	0.2994	0.6696
22.5	1.1025	0.653	0.3361	0.7517
25	1.2229	0.725	0.3728	0.8338
27.5	1.3433	0.796	0.4094	0.9159
30	1.4637	0.867	0.4461	0.998
32.5	1.5841	0.939	0.4828	1.0801
35	1.7045	1.01	0.5195	1.1622
37.5	1.8249	1.081	0.5562	1.2443
40	1.9453	1.153	0.5929	1.3264
42.5	2.0657	1.224	0.6296	1.4084
45	2.1861	1.295	0.6663	1.4905
47.5	2.3065	1.367	0.703	1.5726
50	2.4269	1.438	0.7397	1.6547
52.5	2.5473	1.509	0.7764	1.7368
55	2.6677	1.581	0.8131	1.8189
57.5	2.7881	1.652	0.8498	1.901
60	2.9085	1.723	0.8865	1.9831

Table 3: Flume Conversion Table

Appendix B:

Lift and Drag

Theoretical Calculation of Lift and Drag Forces on Flat Submergence Plane

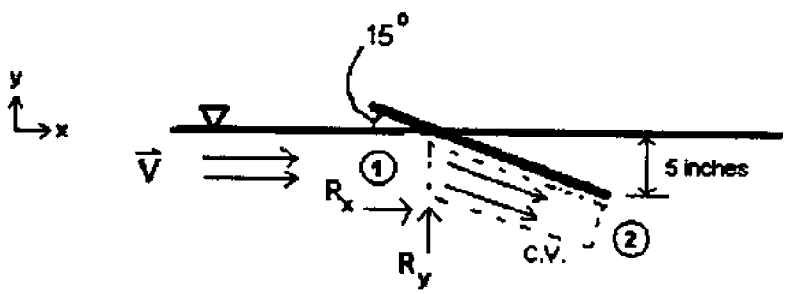

Using control volume analysis

Assumptions
1) Steady Flow
2) Incompressible Flow
3) Uniform Flow

v=velocity $\theta := 15\,deg$

V=volume $knot := 1.68781\frac{ft}{sec}$

Where: v is the velocity of the water
ρ is the density of water
V is the control volume
A is the area of the control volume
F.B is the body force on the control volume
F.S is the surface force on the control volume
u is the magnitude of the relative velocity

$$F_S + F_B = \frac{d}{dt}\int_{cv} v\rho\, dV + \int_{cs} v\rho v\, dA$$

(1) Momentum equation for inertial control volume

$$0 = \frac{d}{dt}\int_{cv} \rho\, dV + \int_{cs} \rho v\, dA$$

(2) Conservation of Mass

0 0 (1)

$$F_{Sx} + F_{Bx} = \frac{d}{dt}\int_{cv} v\rho\, dV + \int_{cs} v\rho v\, dA \qquad (1)$$

$$F_{Sx} = R_x = \int_{A_1} -u\,|\rho v|\,dA + \int_{A_2} u\,|\rho v|\,dA = -u_1\,|\rho v_1 \cdot A_1| + u_2\,|\rho v_2 \cdot A_2|$$

$$0=\frac{d}{dt}\int_{cv}\rho\,dV+\int_{cs}\rho v\,dA \qquad v=\text{constant} \qquad (2)$$

$$0=\int_{A_1}-|\rho v|dA+\int_{A_2}-|\rho v|dA=-|\rho v_1\cdot A_1|+|\rho v_2\cdot A_2|$$

Therefore $\rho v_1\cdot A_1=\rho v_2\cdot A_2$

$R_x=u_2|\rho v_2\cdot A_2|-u_1|\rho v_1\cdot A_1|$

$v_1:=1.5\cdot knot \quad u_2:=v_1\cdot\cos(\theta) \quad u_1:=v_1$

$R_x:=(u_2-u_1)\rho\cdot v_1\cdot A_1$

$A_1:=46\,in\cdot 5\,in \quad \rho:=999\frac{kg}{m^3} \quad v_1=0.772\frac{m}{sec}$

$R_x=-3.008N$

46 is width of tank
5 is draft of plane

$R_x=-0.676\cdot lbf$

---

0 (1)

$$F_{Sy}+F_{By}=\frac{d}{dt}\int_{cv}vp\,dV+\int_{cs}v\rho v\,dA \qquad (1)$$

$F_{Sy}=R_{By} \quad -Mg=F_{By}$

where Mg is the weight of the control volume.

$$R_y-Mg=\int_{cs}v\rho v\,dA=\int_{A_2}u|\rho v|dA=v_2|\rho v_2\cdot A_2| \qquad v_2=-v_1\cdot\sin(\theta)$$

$R_y-Mg=-v\sin(\theta)|\rho v_2\cdot A_2|=-v|\rho v_1\cdot A_1|$

$v_2:=-v_1\cdot\sin(\theta)$

$R_y:=v_2\cdot\rho\cdot v_1\cdot(A_1)\blacksquare+Mg$

$R_y=-22.846N\ \blacksquare+Mg$

$R_y=-5.136\cdot lbf\ \blacksquare+Mg$

Lift and Drag Testing Protocol

The test procedure for the sixteen lift and drag experiments performed followed this general protocol. It is assumed that the submergence plane is installed on the track and the desired configuration of the horizontal baffle and rear boom is complete.

1) Load cell was calibrated sideways using known weights connected to the load cell via a string and a pulley. The multiplier coefficient and intercept constant required for the "QBasic" program were solved for entered into the program and verified against the known weights. The moment arm for the weight was determined from the pivoting point to the center of where the lead bars were added.
2) Tests began at 10 Hertz.
3) Sufficient time was allowed to elapse between input frequency changes to insure uniform velocities in the flume.
4) Lead weights were added and removed as needed to the back of the submergence plane to keep the tail of the submergence plane at the 5 inch draft line.
5) Once the proper amount of weight was determined, the load cell reading was averaged over a period of at least ten seconds. This average load cell value was then recorded.
6) The lead bars were removed from the submergence plane and weighed using an electronic scale. This weight was recorded.
7) The input frequency was bumped up 2.5 Hertz. Procedure returned back to step #3 and was repeated. These experiments ran up to 57.5 Hertz.

Straight Plane Lift and Drag Tests

Tests #12, 13, 14 were used for the Lift and Drag Analysis

Test #12 Mar 25th 11:30:00 AM moment arm = 25 (in) BF + RR

Motor Input Frequency (Hz)	Test-Section Velocity (ft/sec)	Test-Section Velocity (knot)	Load Cell Force (lbm)	Added Weight (lbm)	Moment @ pivot (ft*lbm)	Water Force P (lbm)	Drag Px (lbm)	Lift Py (lbm)	Location x (in)	Reaction Fy (lbm)
0	0	0	0	0	0	0	0	0	0	0
10	0.47	0.27846748	0.33	0.686	1.42917	1.275	0.33	1.232	13.45078	0.545574
12.5	0.57	0.33771588	0.44	0.988	2.05833	1.7	0.44	1.642	14.52919	0.654098
15	0.7	0.4147388	0.6	1.477	3.07708	2.3182	0.6	2.239	15.92819	0.762225
17.5	0.8	0.4739872	0.86	2.07	4.3125	3.3228	0.86	3.21	15.57432	1.139556
20	0.95	0.5628598	1.08	2.504	5.21667	4.1728	1.08	4.031	15.00195	1.526605
22.5	1.08	0.63988272	1.3	2.97	6.1875	5.0228	1.3	4.852	14.78258	1.881654
25	1.22	0.72283048	1.73	3.587	7.47292	6.6842	1.73	6.456	13.41598	2.869432
27.5	1.29	0.76430436	2.06	4.414	9.19583	7.9592	2.06	7.688	13.86444	3.274006
30	1.42	0.84132728	2.25	4.863	10.1313	8.6933	2.25	8.397	13.98489	3.534094
32.5	1.54	0.91242536	2.5	5.481	11.4188	9.6592	2.5	9.33	14.1859	3.849104
35	1.64	0.97167376	3.1	6.876	14.325	11.977	3.1	11.57	14.35197	4.693329
37.5	1.8	1.0664712	3.5	7.637	15.9104	13.523	3.5	13.06	14.11861	5.425146
40	1.9	1.1257196	4.08	8.891	18.5229	15.764	4.08	15.23	14.10028	6.33573
42.5	1.98	1.17311832	4.79	10.108	21.0583	18.507	4.79	17.88	13.65422	7.76848
45	2.13	1.26199092	5.12	11.29	23.5208	19.782	5.12	19.11	14.26794	7.818053
47.5	2.27	1.34493868	5.28	12.838	26.7458	20.4	5.28	19.71	15.73261	6.86718
50	2.46	1.45751064	6.75	14.592	30.4	26.08	6.75	25.19	13.98776	10.59928
52.5	2.55	1.5108342	7.24	15.77	32.8542	27.973	7.24	27.02	14.09387	11.24998
55	2.67	1.58193228	8.03	17.383	36.2146	31.025	8.03	29.97	14.00704	12.58529
57.5	2.79	1.65303036	8.72	18.627	38.8063	33.691	8.72	32.54	13.82177	13.9164
60	stopped									

Test #13 Mar 25th 1:30:00 PM moment arm = 25 (in) BF + RR

Motor Input Frequency (Hz)	Test-Section Velocity (ft/sec)	Test-Section Velocity (knot)	Load Cell Force (lbm)	Added Weight (lbm)	Moment @ pivot (ft*lbm)	Water Force P (lbm)	Drag Px (lbm)	Lift Py (lbm)	Location x (in)	Reaction Fy (lbm)
0	0	0	0	0	0	0	0	0	0	0
10	0.47	0.27846748	0.3	0.694	1.44583	1.1591	0.3	1.12	14.9684	0.425613
12.5	0.57	0.33771588	0.365	0.988	2.05833	1.4102	0.365	1.362	17.51464	0.374195
15	0.7	0.4147388	0.55	1.477	3.07708	2.125	0.55	2.053	17.37621	0.575623
17.5	0.8	0.4739872	0.8	1.75	3.64583	3.091	0.8	2.986	14.1542	1.235633
20	0.95	0.5628598	1.06	2.24	4.66667	4.0955	1.06	3.956	13.67349	1.715964

22.5	1.08	0.63988272	1.24	2.829	5.89375	4.791	1.24	4.628	14.76211	1.798732
25	1.22	0.72283048	1.71	3.508	7.30833	6.6069	1.71	6.382	13.27397	2.873791
27.5	1.29	0.76430436	1.91	4.039	8.41458	7.3797	1.91	7.128	13.68289	3.0892
30	1.42	0.84132728	2.4	5.152	10.7333	9.2729	2.4	8.957	13.88999	3.8049
32.5	1.54	0.91242536	2.65	5.741	11.9604	10.239	2.65	9.89	14.01777	4.14891
35	1.64	0.97167376	2.98	6.603	13.7563	11.514	2.98	11.12	14.33713	4.518484
37.5	1.8	1.0664712	3.63	7.968	16.6	14.025	3.63	13.55	14.20299	5.579311
40	1.9	1.1257196	4.13	8.825	18.3854	15.957	4.13	15.41	13.82617	6.588332
42.5	1.98	1.17311832	4.44	9.758	20.3292	17.155	4.44	16.57	14.22051	6.812265
45	2.13	1.26199092	5.18	11.091	23.1063	20.014	5.18	19.33	13.8541	8.240976
47.5	2.27	1.34493868	5.84	12.5	26.0417	22.564	5.84	21.8	13.84951	9.295123
50	2.46	1.45751064	6.36	13.698	28.9542	24.573	6.36	23.74	14.13945	9.837785
52.5	2.55	1.5108342	7.06	15.386	32.0542	27.278	7.06	26.35	14.10127	10.96221
55	2.67	1.58193228	8.47	16.918	35.2458	32.725	8.47	31.61	12.92418	14.69239
57.5	2.79	1.65303036	9.09	18.093	37.6938	35.121	9.09	33.92	12.87905	15.83126
60 stopped										

Test #14 Mar 25th 5:30:00 PM moment arm = 25 (in) . RR

Motor Input Frequency	Test-Section Velocity	Test-Section Velocity	Load Cell Force	Added Weight	Moment @ pivot	Water Force P	Drag Px	Lift Py	Location x	Reaction Fy
(Hz)	(ft/sec)	(knot)	(lbm)	(lbm)	(ft*lbm)	(lbm)	(lbm)	(lbm)	(in)	(lbm)
0	0	0	0	0	0	0	0	0	0	0
10	0.47	0.27846748	0.3	0.624	1.3	1.1591	0.3	1.12	13.45862	0.495613
12.5	0.57	0.33771588	0.41	0.853	1.77708	1.5841	0.41	1.53	13.46178	0.677137
15	0.7	0.4147388	0.61	1.215	2.53125	2.3569	0.61	2.277	12.88795	1.061545
17.5	0.8	0.4739872	0.84	1.713	3.56875	3.2455	0.84	3.135	13.19518	1.421915
20	0.95	0.5628598	1.01	2.077	4.32708	3.9023	1.01	3.769	13.30615	1.692362
22.5	1.08	0.63988272	1.43	2.919	6.08125	5.5251	1.43	5.337	13.20795	2.41782
25	1.22	0.72283048	1.66	3.51	7.3125	6.4137	1.66	6.195	13.68158	2.685189
27.5	1.29	0.76430436	1.93	4.094	8.52917	7.4569	1.93	7.203	13.72549	3.10884
30	1.42	0.84132728	2.25	4.952	10.3167	8.6933	2.25	8.397	14.24083	3.445094
32.5	1.54	0.91242536	2.4	5.267	10.9729	9.2729	2.4	8.957	14.20003	3.6899
35	1.64	0.97167376	3	6.523	13.5896	11.591	3	11.2	14.069	4.673125
37.5	1.8	1.0664712	3.49	7.549	15.7271	13.484	3.49	13.02	13.99591	5.475825
40	1.9	1.1257196	3.95	8.358	17.4125	15.262	3.95	14.74	13.69123	6.383565
42.5	1.98	1.17311832	4.55	9.804	20.425	17.58	4.55	16.98	13.94213	7.17679
45	2.13	1.26199092	5.06	10.745	22.3854	19.55	5.06	18.88	13.7402	8.139131
47.5	2.27	1.34493868	5.52	12.004	25.0083	21.328	5.52	20.6	14.07097	8.59687
50	2.46	1.45751064	6.37	13.512	28.15	24.612	6.37	23.77	13.72516	10.26111
52.5	2.55		6.98	14.967	31.1813	26.969	6.98	26.05	13.87448	11.08265
55	2.67		7.9	16.771	34.9396	30.523	7.9	29.48	13.73628	12.71213
57.5	2.79		8.14	17.884	37.2583	31.45	8.14	30.38	14.216	12.49482
60 stopped										

The following tests were not used in the Lift and Drag Analysis, because gap geometries and the horizontal baffle had been changed from the plywood baffle to the PVC baffle

Test #1 Feb 24th 5:30:00 PM moment arm = 24.5 (in) BF + RR

Motor Input Frequency (Hz)	Test-Section Velocity (ft/sec)	Test-Section Velocity (knot)	Load Cell Force (lbm)	Added Weight (lbm)	Moment @ pivot (ft*lbm)	Water Force P (lbm)	Drag Px (lbm)	Lift Py (lbm)	Location x (in)	Reaction Fy (lbm)
0	0	0	0.02	0	0	0.0773	0.02	0.075	0	0.074641
10	0.47	0.27846748	0.43	0.683	1.39446	1.6614	0.43	1.605	10.072	0.921778
20	0.95	0.5628598	1.08	2.132	4.35283	4.1728	1.08	4.031	12.51776	1.898605
30	1.42	0.84132728	2.51	4.691	9.57746	9.6979	2.51	9.367	11.851	4.676425
40	1.9	1.1257196	5	9.145	18.671	19.318	5	18.66	11.59784	9.515208
50	2.46	1.45751064	8	14.859	30.3371	30.91	8	29.86	11.77777	14.99733
55	stopped									

Test #2 Feb 25th 12:30:00 PM moment arm = 24.5 (in) BF

Motor Input Frequency (Hz)	Test-Section Velocity (ft/sec)	Test-Section Velocity (knot)	Load Cell Force (lbm)	Added Weight (lbm)	Moment @ pivot (ft*lbm)	Water Force P (lbm)	Drag Px (lbm)	Lift Py (lbm)	Location x (in)	Reaction Fy (lbm)
0	0	0	0	0	0	0	0	0	0	0
10	0.47	0.27846748	0.7	0.7	1.42917	2.7046	0.7	2.612	6.341081	1.912429
15	0.7	0.4147388	0.537	1.065	2.17438	2.0748	0.537	2.004	12.57589	0.939106
20	0.95	0.5628598	0.96	1.964	4.00983	3.7091	0.96	3.583	12.9728	1.61876
25	1.22	0.72283048	1.505	3.219	6.57213	5.8149	1.505	5.617	13.56275	2.397723
30	1.42	0.84132728	2.68	4.791	9.78163	10.355	2.68	10	11.33587	5.210872
35	1.64	0.97167376	3.55	6.36	12.985	13.716	3.55	13.25	11.36036	6.888748
40	1.9	1.1257196	4.72	8.448	17.248	18.237	4.72	17.62	11.34946	9.167237
45	2.13	1.26199092	6.1	11.266	23.0014	23.569	6.1	22.77	11.71125	11.49945
50	stopped									

Test #3 Feb 25th 2:00:00 PM moment arm = 24.5 (in) BF

Motor Input Frequency (Hz)	Test-Section Velocity (ft/sec)	Test-Section Velocity (knot)	Load Cell Force (lbm)	Added Weight (lbm)	Moment @ pivot (ft*lbm)	Water Force P (lbm)	Drag Px (lbm)	Lift Py (lbm)	Location x (in)	Reaction Fy (lbm)
0	0	0	0	0	0	0	0	0	0	0
10	0.47	0.27846748	0.5	0.534	1.09025	1.9318	0.5	1.866	6.772275	1.332021
15	0.7	0.4147388	0.83	1.235	2.52146	3.2069	0.83	3.098	9.435223	1.862595
20	0.95	0.5628598	1.48	2.321	4.73871	5.7183	1.48	5.523	9.944358	3.202422
25	1.22	0.72283048	1.79	3.023	6.17196	6.916	1.79	6.68	10.70899	3.657355
30	1.42	0.84132728	2.59	4.7	9.59583	10.007	2.59	9.666	11.50698	4.965988
35	1.64	0.97167376	3.39	5.979	12.2071	13.098	3.39	12.65	11.18387	6.672621
40	1.9	1.1257196	5.07	8.803	17.9728	19.589	5.07	18.92	11.00997	10.11845
45	2.13	1.26199092	6.2	11.233	22.934	23.955	6.2	23.14	11.48861	11.90566
50	stopped									

Test #6 Mar 3rd 12:30:00 PM moment arm = 24.5 (in) BF + DS

Motor Input Frequency (Hz)	Test-Section Velocity (ft/sec)	Test-Section Velocity (knot)	Load Cell Force (lbm)	Added Weight (lbm)	Moment @ pivot (ft*lbm)	Water Force P (lbm)	Drag Px (lbm)	Lift Py (lbm)	Location x (in)	Reaction Fy (lbm)
0	0	0	0	0	0	0	0	0	0	0
10	0.47	0.27846748	0.23	0.624	1.274	0.8886	0.23	0.858	17.20363	0.23437
12.5	0.57	0.33771588	0.265	0.745	1.52104	1.0239	0.265	0.989	17.82681	0.243991
15	0.7	0.4147388	0.345	1.113	2.27238	1.333	0.345	1.288	20.45688	0.174554
17.5	0.8	0.4739872	0.59	1.704	3.479	2.2796	0.59	2.202	18.3139	0.497905
20	0.95	0.5628598	0.74	2.077	4.24054	2.8591	0.74	2.762	17.79787	0.684711
22.5	1.08	0.63988272	0.91	2.392	4.88367	3.516	0.91	3.396	16.66798	1.004158
25	1.22	0.72283048	1.27	3.254	6.64358	4.9069	1.27	4.74	16.24715	1.485693
27.5	1.29	0.76430436	1.5	4.004	8.17483	5.7955	1.5	5.598	16.92646	1.594063
30	1.42	0.84132728	1.92	4.711	9.61829	7.4183	1.92	7.166	15.55877	2.45452
32.5	1.54	0.91242536	2.31	5.529	11.2884	8.9251	2.31	8.621	15.17742	3.092016
35	1.64	0.97167376	2.65	6.451	13.1708	10.239	2.65	9.89	15.43634	3.43891
37.5	1.8	1.0664712	2.85	7.035	14.3631	11.012	2.85	10.64	15.65246	3.601319
40	1.9	1.1257196	3.18	7.833	15.9924	12.287	3.18	11.87	15.6194	4.034893
42.5	1.98	1.17311832	3.95	9.535	19.4673	15.262	3.95	14.74	15.30689	5.206565
45	2.13	1.26199092	4.2	10.121	20.6637	16.228	4.2	15.67	15.2805	5.553575
47.5	2.27	1.34493868	4.75	11.468	23.4138	18.353	4.75	17.73	15.30937	6.259198
50	2.46	1.45751064	5.3	13.113	26.7724	20.478	5.3	19.78	15.68879	6.666821
52.5	2.55	1.5108342	6.3	15.027	30.6801	24.341	6.3	23.51	15.12499	8.484863
55	2.67	1.58193228	7	16.687	34.0693	27.046	7	26.12	15.11623	9.437292
57.5	2.79	1.65303036	7.3	17.54	35.8108	28.205	7.3	27.24	15.23597	9.703904
60	stopped									

Convex Plane Lift and Drag Tests

Tests #9, 10, 11 were used for the Lift and Drag Analysis

Test #9 Mar 23rd 1:00:00 PM moment arm = 22 (in) BF + RR

Motor Input Frequency (Hz)	Test-Section Velocity (ft/sec)	Test-Section Velocity (knot)	Load Cell Force (lbm)	Added Weight (lbm)	Moment @ pivot (ft*lbm)	Water Force P (lbm)	Drag Px (lbm)	Lift Py (lbm)	Location x (in)	Reaction Fy (lbm)
0	0	0	0	0	0	0	0	0	0	0
10	0.47	0.27846748	0.145	0.489	0.8965	0.5602	0.145	0.541	19.2026	0.052146
12.5	0.57	0.33771588	0.15	0.853	1.56383	0.5796	0.15	0.56	32.3801	-0.29319
15	0.7	0.4147388	0.25	1.257	2.3045	0.9659	0.25	0.933	28.6296	-0.32399
17.5	0.8	0.4739872	1.1	1.854	3.399	4.2501	1.1	4.105	9.59703	2.251246
20	0.95	0.5628598	1.3	2.599	4.76483	5.0228	1.3	4.852	11.3837	2.252654
22.5	1.08	0.63988272	1.7	3.109	5.69983	6.5683	1.7	6.344	10.4134	3.235471
25	1.22	0.72283048	2.3	4.297	7.87783	8.8865	2.3	8.584	10.6379	4.286696
27.5	1.29	0.76430436	2.6	5.152	9.44533	10.046	2.6	9.703	11.2829	4.551308
30	1.42	0.84132728	2.9	6.005	11.0092	11.205	2.9	10.82	11.7906	4.817921
32.5	1.54	0.91242536	3.5	7.225	13.2458	13.523	3.5	13.06	11.7541	5.837146
35	1.64	0.97167376	4.3	8.43	15.455	16.614	4.3	16.05	11.163	7.617779
37.5	1.8	1.0664712	4.6	9.054	16.599	17.773	4.6	17.17	11.2073	8.113392
40	1.9	1.1257196	5.3	10.229	18.7532	20.478	5.3	19.78	10.9895	9.550821
42.5	1.98	1.17311832	5.8	11.473	21.0338	22.409	5.8	21.65	11.2634	10.17284
45	2.13	1.26199092	6.9	13.735	25.1808	26.659	6.9	25.75	11.3344	12.01609
47.5	2.27	1.34493868	8.1	16.074	29.469	31.296	8.1	30.23	11.2995	14.15554
50	2.46	1.45751064	8.7	17.2	31.5333	33.614	8.7	32.47	11.2572	15.26876
52.5	2.55	1.5108342	9.8	19.244	35.2807	37.864	9.8	36.57	11.1812	17.33001
55	stopped									

Test #10 Mar 23rd 3:00:00 PM moment arm = 22 (in) RR

Motor Input Frequency (Hz)	Test-Section Velocity (ft/sec)	Test-Section Velocity (knot)	Load Cell Force (lbm)	Added Weight (lbm)	Moment @ pivot (ft*lbm)	Water Force P (lbm)	Drag Px (lbm)	Lift Py (lbm)	Location x (in)	Reaction Fy (lbm)
0	0	0	0	0	0	0	0	0	0	0
10	0.47	0.27846748	0.14	0.489	0.8965	0.5409	0.14	0.522	19.8884	0.033486
12.5	0.57	0.33771588	0.46	0.591	1.0835	1.7773	0.46	1.717	7.31559	1.125739
15	0.7	0.4147388	0.85	1.127	2.06617	3.2841	0.85	3.172	7.54962	2.045235
17.5	0.8	0.4739872	1.1	1.876	3.43933	4.2501	1.1	4.105	9.71091	2.229246
20	0.95	0.5628598	1.55	2.52	4.62	5.9887	1.55	5.785	9.25739	3.264665
22.5	1.08	0.63988272	1.8	3.545	6.49917	6.9547	1.8	6.718	11.2141	3.172675
25	1.22	0.72283048	2.3	4.297	7.87783	8.8865	2.3	8.584	10.6379	4.286696

27.5	1.29	0.76430436	2.7	4.833	8.8605	10.432	2.7	10.08	10.1923	5.243513
30	1.42	0.84132728	3.25	5.972	10.9487	12.557	3.25	12.13	10.463	6.157135
32.5	1.54	0.91242536	3.8	7.145	13.0992	14.682	3.8	14.18	10.7063	7.036758
35	1.64	0.97167376	4.3	8.281	15.1818	16.614	4.3	16.05	10.9656	7.766779
37.5	1.8	1.0664712	4.95	9.486	17.391	19.125	4.95	18.47	10.9118	8.987606
40	1.9	1.1257196	5.6	10.567	19.3728	21.637	5.6	20.9	10.7444	10.33243
42.5	1.98	1.17311832	6.2	11.958	21.923	23.955	6.2	23.14	10.9821	11.18066
45	2.13	1.26199092	7.1	13.728	25.168	27.432	7.1	26.5	11.0095	12.7695
47.5	2.27	1.34493868	8	15.331	28.1068	30.91	8	29.86	10.9119	14.52533
50	2.46	1.45751064	8.8	17.734	32.5123	34.001	8.8	32.84	11.4748	15.10797
52.5	2.55	1.5108342	10.1	19.835	36.3642	39.023	10.1	37.69	11.1823	17.85862
55	stopped									

Test #11 Mar 23rd 5:00:00 PM moment arm = 22 (in) RR

Motor Input Frequency (Hz)	Test-Section Velocity (ft/sec)	Test-Section Velocity (knot)	Load Cell Force (lbm)	Added Weight (lbm)	Moment @ pivot (ft*lbm)	Water Force P (lbm)	Drag Px (lbm)	Lift Py (lbm)	Location x (in)	Reaction Fy (lbm)
0	0	0	0	0	0	0	0	0	0	0
10	0.47	0.27846748	0.17	0.337	0.61783	0.6568	0.17	0.634	11.2876	0.297447
12.5	0.57	0.33771588	0.71	0.591	1.0835	2.7432	0.71	2.65	4.73968	2.05875
15	0.7	0.4147388	0.89	1.08	1.98	3.4387	0.89	3.322	6.90961	2.241517
17.5	0.8	0.4739872	1.15	1.883	3.45217	4.4432	1.15	4.292	9.32336	2.408848
20	0.95	0.5628598	1.5	2.474	4.53567	5.7955	1.5	5.598	9.39136	3.124063
22.5	1.08	0.63988272	1.91	3.007	5.51283	7.3797	1.91	7.128	8.96437	4.1212
25	1.22	0.72283048	2.3	4.167	7.6395	8.8865	2.3	8.584	10.3161	4.416696
27.5	1.29	0.76430436	2.7	4.766	8.73767	10.432	2.7	10.08	10.051	5.310513
30	1.42	0.84132728	3.3	6.03	11.055	12.75	3.3	12.32	10.4045	6.285738
32.5	1.54	0.91242536	3.9	7.286	13.3577	15.068	3.9	14.55	10.6376	7.268963
35	1.64	0.97167376	4.4	8.144	14.9307	17	4.4	16.42	10.5391	8.276983
37.5	1.8	1.0664712	4.9	8.889	16.2965	18.932	4.9	18.29	10.3294	9.398004
40	1.9	1.1257196	5.5	10.117	18.5478	21.25	5.5	20.53	10.4739	10.40923
42.5	1.98	1.17311832	6.3	12.059	22.1082	24.341	6.3	23.51	10.8991	11.45286
45	2.13	1.26199092	7	14.043	25.7455	27.046	7	26.12	11.423	12.08129
47.5	2.27	1.34493868	8	15.984	29.304	30.91	8	29.86	11.3767	13.87233
50	2.46	1.45751064	9.1	17.694	32.439	35.16	9.1	33.96	11.0715	16.26758
52.5	2.55	1.5108342	9.9	19.632	35.992	38.251	9.9	36.95	11.2914	17.31521
55	stopped									

Test #8 Mar 5th 5:30:00 PM moment arm = 22 (in) BF

Motor Input Frequency (Hz)	Test-Section Velocity (ft/sec)	Test-Section Velocity (knot)	Load Cell Force (lbm)	Added Weight (lbm)	Moment @ pivot (ft*lbm)	Water Force P (lbm)	Drag Px (lbm)	Lift Py (lbm)	Location x (in)	Reaction Fy (lbm)
0	0	0	0	0	0	0	0	0	0	0
10	0.47	0.27846748	0.42	0.886	1.62433	1.6228	0.42	1.567	12.0117	0.681458
12.5	0.57	0.33771588	0.52	1.248	2.288	2.0091	0.52	1.941	13.6657	0.692662
15	0.7	0.4147388	0.56	1.612	2.95533	2.1637	0.56	2.09	16.3907	0.477943
17.5	0.8	0.4739872	0.79	2.385	4.3725	3.0523	0.79	2.948	17.1902	0.563313
20	0.95	0.5628598	1.08	2.829	5.1865	4.1728	1.08	4.031	14.9152	1.201605
22.5	1.08	0.63988272	1.34	3.556	6.51933	5.1774	1.34	5.001	15.1104	1.444936
25	1.22	0.72283048	1.74	4.288	7.86133	6.7228	1.74	6.494	14.0322	2.205753
27.5	1.29	0.76430436	2.25	5.256	9.636	8.6933	2.25	8.397	13.3013	3.141094
30	1.42	0.84132726	2.46	5.926	10.8643	9.5047	2.46	9.181	13.7166	3.254823
32.5	1.54	0.91242536	2.9	6.982	12.8003	11.205	2.9	10.82	13.7089	3.840921
35	1.64	0.97167376	3.39	8.225	15.0792	13.098	3.39	12.65	13.8152	4.426621
37.5	1.8	1.0664712	3.96	9.226	16.9143	15.3	3.96	14.78	13.2659	5.552885
40	1.9	1.1257196	4.45	10.318	18.9163	17.193	4.45	16.61	13.2025	6.289585
42.5	1.98	1.17311832	5.09	11.702	21.4537	19.666	5.09	19	13.0907	7.294092
45	2.13	1.26199092	5.84	13.528	24.8013	22.564	5.84	21.8	13.1899	8.267123
47.5	2.27	1.34493868	6.32	14.742	27.027	24.419	6.32	23.59	13.2819	8.844503
50	2.46	1.45751064	7.08	16.524	30.294	27.355	7.08	26.42	13.2893	9.898855
52.5	2.55	1.5108342	7.95	18.263	33.4822	30.716	7.95	29.67	13.0805	11.40673
55	2.67	1.58193228	9.06	20.644	37.8473	35.005	9.06	33.81	12.9743	13.1683
57.5 stopped										

Test #8 was not used in the lift and drag analysis, because the horizontal baffle changed from the plywood baffle to the PVC.

Concave ("J") Plane Lift and Drag Tests

Tests #15 and #16 were used for the Lift and Drag Analysis.

Test #15 Mar 26th 7:00:00 PM moment arm = 33 (in) BF + RR

Motor Input Frequency (Hz)	Test-Section Velocity (ft/sec)	Test-Section Velocity (knot)	Load Cell Force (lbm)	Added Weight (lbm)	Moment @ pivot (ft*lbm)	Water Force P (lbm)	Drag Px (lbm)	Lift Py (lbm)	Location x (in)	Reaction Fy (lbm)
0	0	0	0	0	0	0	0	0	0	0
10	0.47	0.27846748	0.17	0.363	0.99825	0.6568	0.17	0.634	18.2376	0.271447
12.5	0.57	0.33771588	0.25	0.492	1.353	0.9659	0.25	0.933	16.8088	0.44101
15	0.7	0.4147388	0.32	0.536	1.474	1.2364	0.32	1.194	14.3063	0.658253
17.5	0.8	0.4739872	0.5	0.853	2.34575	1.9318	0.5	1.866	14.571	1.013021
20	0.95	0.5628598	0.64	0.899	2.47225	2.4728	0.64	2.389	11.9975	1.489507
22.5	1.08	0.63988272	0.96	1.219	3.35225	3.7091	0.96	3.583	10.8454	2.36376
25	1.22	0.72283048	1.15	1.345	3.69875	4.4432	1.15	4.292	9.98931	2.946848
27.5	1.29	0.76430436	1.42	1.453	3.99575	5.4864	1.42	5.299	8.73954	3.846499
30	1.42	0.84132728	1.69	1.581	4.34775	6.5296	1.69	6.307	7.99018	4.72615
32.5	1.54	0.91242536	2.03	1.79	4.9225	7.8433	2.03	7.576	7.53127	5.786045
35	1.64	0.97167376	2.47	2.156	5.929	9.5433	2.47	9.218	7.45526	7.062143
37.5	1.8	1.0664712	2.92	2.346	6.4515	11.282	2.92	10.9	6.86209	8.551562
40	1.9	1.1257196	3.16	2.498	6.8695	12.209	3.16	11.79	6.75175	9.295252
42.5	1.98	1.17311832	3.71	3.032	8.338	14.334	3.71	13.85	6.98018	10.81387
45	2.13	1.26199092	4.25	3.355	9.22625	16.421	4.25	15.86	6.7424	12.50618
47.5	2.27	1.34493868	4.81	3.675	10.1063	18.584	4.81	17.95	6.52564	14.27612
50	2.46	1.45751064	5.42	4.211	11.5803	20.941	5.42	20.23	6.63586	16.01667
52.5	2.55	1.5108342	5.55	4.211	11.5803	21.444	5.55	20.71	6.48042	16.50183
55	2.67	1.58193228	6.05	4.528	12.452	23.375	6.05	22.58	6.39237	18.05085
57.5	2.79	1.65303036	6.62	4.7	12.925	25.578	6.62	24.71	6.06389	20.00612
60	stopped									

Test #16 Mar 26th 10:00:00 PM moment arm = 33 (in) BF + RR

Motor Input Frequency (Hz)	Test-Section Velocity (ft/sec)	Test-Section Velocity (knot)	Load Cell Force (lbm)	Added Weight (lbm)	Moment @ pivot (ft*lbm)	Water Force P (lbm)	Drag Px (lbm)	Lift Py (lbm)	Location x (in)	Reaction Fy (lbm)
0	0	0	0	0	0	0	0	0	0	0
10	0.47	0.27846748	0.2	0.364	1.001	0.7727	0.2	0.746	15.5447	0.382408
12.5	0.57	0.33771588	0.26	0.624	1.716	1.0046	0.26	0.97	20.4985	0.346331
15	0.7	0.4147388	0.36	756	2079	1.3909	0.36	1.344	17936.2	-754.656
17.5	0.8	0.4739872	0.48	0.911	2.50525	1.8546	0.48	1.791	16.2102	0.88038

20	0.95	0.5628598	0.62	1.116	3.069	2.3955	0.62	2.314	15.3739	1.197866
22.5	1.08	0.63988272	0.77	1.12	3.08	2.975	0.77	2.874	12.4233	1.753672
25	1.22	0.72283048	1.02	1.292	3.553	3.941	1.02	3.807	10.8187	2.514683
27.5	1.29	0.76430436	1.32	1.418	3.8995	5.1001	1.32	4.926	9.17516	3.508295
30	1.42	0.84132728	1.68	1.486	4.0865	6.491	1.68	6.27	7.55476	4.78383
32.5	1.54	0.91242536	2.07	1.72	4.73	7.9978	2.07	7.725	7.09691	6.005326
35	1.64	0.97167376	2.39	2.083	5.72825	9.2342	2.39	8.92	7.44393	6.83658
37.5	1.8	1.0664712	2.8	2.253	6.19575	10.818	2.8	10.45	6.87249	8.196717
40	1.9	1.1257196	3.15	2.575	7.08125	12.171	3.15	11.76	6.98197	9.180931
42.5	1.98	1.17311832	3.79	3.115	8.56625	14.643	3.79	14.14	7.01989	11.02944
45	2.13	1.26199092	4.14	3.296	9.064	15.996	4.14	15.45	6.79983	12.15465
47.5	2.27	1.34493868	4.31	3.607	9.91925	16.653	4.31	16.09	7.14793	12.4781
50	2.46	1.45751064	5.09	4.076	11.209	19.666	5.09	19	6.83955	14.92009
52.5	2.55	1.5108342	5.62	4.61	12.6775	21.714	5.62	20.97	7.00609	16.36407
55	2.67	1.58193228	6.42	4.773	13.1258	24.805	6.42	23.96	6.34991	19.18671
57.5	2.79	1.65303036	6.42	4.976	13.684	24.805	6.42	23.96	6.61998	18.98371
60 stopped										

The following tests were not used for analysis because of changes made to the gap geometries and the horizontal baffle.

Test #4 01-Mar 11:30:00 PM moment arm = 31 (in) BF

Motor Input Frequency (Hz)	Test-Section Velocity (ft/sec)	Test-Section Velocity (knot)	Load Cell Force (lbm)	Added Weight (lbm)	Moment @ pivot (ft*lbm)	Water Force P (lbm)	Drag Px (lbm)	Lift Py (lbm)	Location x (in)	Reaction Fy (lbm)
0	0	0	0	0	0	0	0	0	0	0
10	0.47	0.27846748	0.455	0.487	1.25808	1.758	0.455	1.698	8.58769	1.211079
15	0.7	0.4147388	0.75	0.851	2.19842	2.8978	0.75	2.799	9.10389	1.948031
20	0.95	0.5628598	1.27	1.124	2.90367	4.9069	1.27	4.74	7.10103	3.615693
25	1.22	0.72283048	1.95	1.623	4.19275	7.5342	1.95	7.277	6.67794	5.654481
30	1.42	0.84132728	2.86	2.308	5.96233	11.05	2.86	10.67	6.47483	8.365639
35	1.64	0.97167376	3.8	2.864	7.39867	14.682	3.8	14.18	6.04712	11.31776
40	1.9	1.1257196	5.3	3.951	10.2067	20.478	5.3	19.78	5.98122	15.82882
45	2.13	1.26199092	7.1	5.218	13.4798	27.432	7.1	26.5	5.89664	21.2795
50	2.46	1.45751064	8.5	6.426	16.6005	32.841	8.5	31.72	6.0657	25.29635
55 stopped										

Test #5 02-Mar 12:30:00 AM moment arm = 31 (in) BF

Motor Input Frequency (Hz)	Test-Section Velocity (ft/sec)	Test-Section Velocity (knot)	Load Cell Force (lbm)	Added Weight (lbm)	Moment @ pivot (ft*lbm)	Water Force P (lbm)	Drag Px (lbm)	Lift Py (lbm)	Location x (in)	Reaction Fy (lbm)
0	0	0	0	0	0	0	0	0	0	0
10	0.47	0.27846748	0.348	0.364	0.94033	1.3446	0.348	1.299	8.3923	0.934751
15	0.7	0.4147388	0.795	0.955	2.46708	3.0716	0.795	2.967	9.63818	2.011973
20	0.95	0.5628598	1.28	1.206	3.1155	4.9455	1.28	4.777	7.55955	3.571013
25	1.22	0.72283048	2.13	1.616	4.17467	8.2297	2.13	7.949	6.08724	6.333249
30	1.42	0.84132728	2.78	2.15	5.55417	10.741	2.78	10.38	6.20515	8.225076
35	1.64	0.97167376	3.8	3.018	7.7965	14.682	3.8	14.18	6.37227	11.16376
40	1.9	1.1257196	5.26	3.882	10.0285	20.323	5.26	19.63	5.92146	15.74854
45	2.13	1.26199092	6.7	5.075	13.1104	25.887	6.7	25	6.07743	19.92968
50	2.46	1.45751064	8.2	6.252	16.151	31.682	8.2	30.6	6.11736	24.35074
55 stopped										

Test #7 05-Mar 3:30:00 PM moment arm = 33 (in) BF

Motor Input Frequency (Hz)	Test-Section Velocity (ft/sec)	Test-Section Velocity (knot)	Load Cell Force (lbm)	Added Weight (lbm)	Moment @ pivot (ft*lbm)	Water Force P (lbm)	Drag Px (lbm)	Lift Py (lbm)	Location x (in)	Reaction Fy (lbm)
0	0	0	0	0	0	0	0	0	0	0
10	0.47	0.27846748	0.23	0.139	0.38225	0.8886	0.23	0.858	5.16176	0.71937
12.5	0.57	0.33771588	0.4	0.364	1.001	1.5455	0.4	1.493	7.77235	1.128817
15	0.7	0.4147388	0.57	0.591	1.62525	2.2023	0.57	2.127	8.85572	1.536264
17.5	0.8	0.4739872	0.67	0.591	1.62525	2.5887	0.67	2.5	7.53397	1.909468
20	0.95	0.5628598	0.92	0.856	2.354	3.5546	0.92	3.433	7.94689	2.577478
22.5	1.08	0.63988272	1.21	1.219	3.35225	4.6751	1.21	4.516	8.60458	3.29677
25	1.22	0.72283048	1.41	1.45	3.9875	5.4478	1.41	5.262	8.78335	3.812179
27.5	1.29	0.76430436	1.65	1.517	4.17175	6.3751	1.65	6.158	7.85259	4.640869
30	1.42	0.84132728	1.95	1.702	4.6805	7.5342	1.95	7.277	7.4548	5.575481
32.5	1.54	0.91242536	2.32	1.967	5.40925	8.9638	2.32	8.658	7.24148	6.691337
35	1.64	0.97167376	2.75	2.238	6.1545	10.625	2.75	10.26	6.95086	8.025115
37.5	1.8	1.0664712	3.18	2.558	7.0345	12.287	3.18	11.87	6.87044	9.309893
40	1.9	1.1257196	3.69	2.558	7.0345	14.257	3.69	13.77	5.92087	11.21323
42.5	1.98	1.17311832	4.1	2.867	7.88425	15.841	4.1	15.3	5.97248	12.43437
45	2.13	1.26199092	4.7	3.23	8.8825	18.159	4.7	17.54	5.8697	14.3106
47.5	2.27	1.34493868	5.15	3.554	9.7735	19.898	5.15	19.22	5.89415	15.66601
50	2.46	1.45751064	5.5	3.918	10.7745	21.25	5.5	20.53	6.08433	16.60823
52.5	2.55	1.5108342	5.9	4.41	12.1275	22.796	5.9	22.02	6.38407	17.60905
55 stopped										

Appendix C:

Bead Testing

Bead Testing Protocol

The following protocol was standard procedure for the bead testing experiments.

1) Flume brought to desired test speed (52.2 Hz) and allowed to develop for at least 90 seconds to insure the achievement of a uniform 1.5 knots (2.53 ft/sec).
2) (T = 0 sec) Began test; 3000 ml of plastic beads poured uniformly into flume tank just after the PVC flow straighteners.
3) (T = 10 sec) Bead dumping halted.
4) (T = 16 sec) Motors stopped abruptly. Beads from the dump should be (or close to being) past the submergence plane. Barrier secured in front of submergence plane to insure no "second chance" for the lost beads from the first pass.[1]
5) (T = 27 sec) Lost beads will have completed one revolution.
5) Test completed – beads collected beginning with the contained region, then any lost beads are collected. Beads are then dried overnight and volumetrically measured the next day.[2]

1 Barrier not introduced until after the initial bead test, when deemed necessary.

2 Wet beads supposedly settle differently than dried beads. The beads began the test dry, so they are dried afterwards to be consistent.